JOURNAL OF MATERIALS SCIENCE 29 (1994) 6354–6378

Anisotropic etching of silicon crystals in KOH solution

Part II *Theoretical two-dimensional etched shapes: discussion of the adequation of the dissolution slowness surface*

C. R. TELLIER, A. BRAHIM-BOUNAB
Laboratoire de Chronométrie Electronique et Piézoélectricité, Ecole Nationale Supérieure de Mécanique et des Microtechniques, La Bouloie, Route de Gray, 25030 Besancon Cedex, France

Theoretical two-dimensional etched shapes are derived from numerical simulations involving the equation of the dissolution slowness surface related to silicon crystals etched in aqueous KOH solutions. Theoretical changes in cross-sectional shapes of starting circular sections and in x'_1 and [0 0 1] profilometry traces with the angle of cut, φ_0, are analysed in terms of the geometrical features of the slowness surface. The important role played by extrema in the dissolution slowness in determining the final two-dimensional etched shapes, is outlined. Theoretical etched shapes are systematically compared with the experimental shapes and the adequation of the proposed slowness surface is discussed.

1. Introduction

During the last three decades, a number of works [1–12] have been devoted to the prediction of etching shapes for starting circular sections [3, 4, 7–11] or for cross-sectional shapes encountered in localized chemical etching at the edge of an inert mask [1, 2, 5–7, 10, 12]. Many investigators [1, 2, 3–6] have based their works on the two dissolution criteria stated by Batterman [13] or on the kinematic model proposed by Frank [4]. Under these conditions only limiting shapes have been constructed geometrically. These shapes are composed of the limiting linear profile elements associated with corresponding extrema in the polar plot of the etch rate, R, versus orientation (i.e. with minima in R for concave profiles or with maxima for convex profiles [4]). Thus the development of rounded portions in cross-sectional sections cannot be treated easily using conventional geometrical procedures.

However, as soon as a model [15, 16] gives us an analytical expression which describes variations in the dissolution slowness, $L(\varphi, \theta) = 1/R$, with the orientation (φ, θ) of crystal plates, it becomes possible [7–12, 17,18] to predict numerically final dissolution shapes in which curved portions must be accounted for. The tensorial representation [15, 16] of anisotropic etching proposed by Tellier and co-workers offers such a possibility, provided the representative surface of the dissolution slowness vector, $\boldsymbol{L}$, was determined from experiments with a sufficient accuracy [8].

In Part I [19] of this work, experiments on the anisotropic etching of silicon crystal circular plates were extensively presented and a procedure to derive the dissolution slowness surface was proposed. In Part II we discuss the adequation of the derived slowness surface by comparing systematically the experimental and theoretical two-dimensional cross-sectional shapes resulting from etching. For this purpose, numerical procedures have been developed which start with polar diagrams of the dissolution slowness. In addition, theoretical etching shapes are analysed in terms of the influence of extrema in the polar plot of $\boldsymbol{L}$.

2. Theoretical basis

2.1. Kinematic description of the anisotropic dissolution

Let us recall that in the three-dimensional description of anisotropic etching [16, 17] the surface of a crystal can be decomposed into a succession of oriented planar surface elements, $\mathbf{ds}$. The orientation of a surface element, is defined by means of two angles of cut, φ and θ, as specified by the IEEE standard on piezoelectricity [20]. To each surface element we associate a dissolution slowness vector, $\boldsymbol{L}$, whose magnitude, $L(\varphi, \theta)$, is the reciprocal of the normal dissolution rate, $R(\varphi, \theta)$, and whose positive direction coincides with that of the inward normal unit vector, $\boldsymbol{n}$, to the surface element (Fig. 1a). As the angles of cut φ and θ vary, the vector $\boldsymbol{L}$ describes in space a representative surface called the dissolution slowness surface.

The magnitude, $L(\varphi, \theta)$, is related to the three cartesian components, n_1, n_2 and n_3, of $\boldsymbol{n}$ by means of a polynomial regression involving components, D_0, D_i,

0022–2461

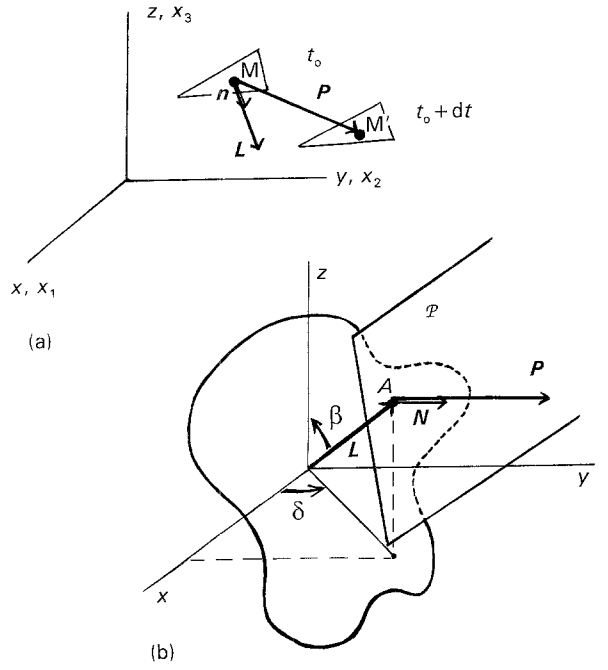

Figure 1 The geometry of the model. (a) Definition of the dissolution slowness vector $\boldsymbol{L}$ and of the propagation vector $\boldsymbol{P}$. (b) Geometrical properties of the propagation vector $\boldsymbol{P}$ in a three-dimensional model.

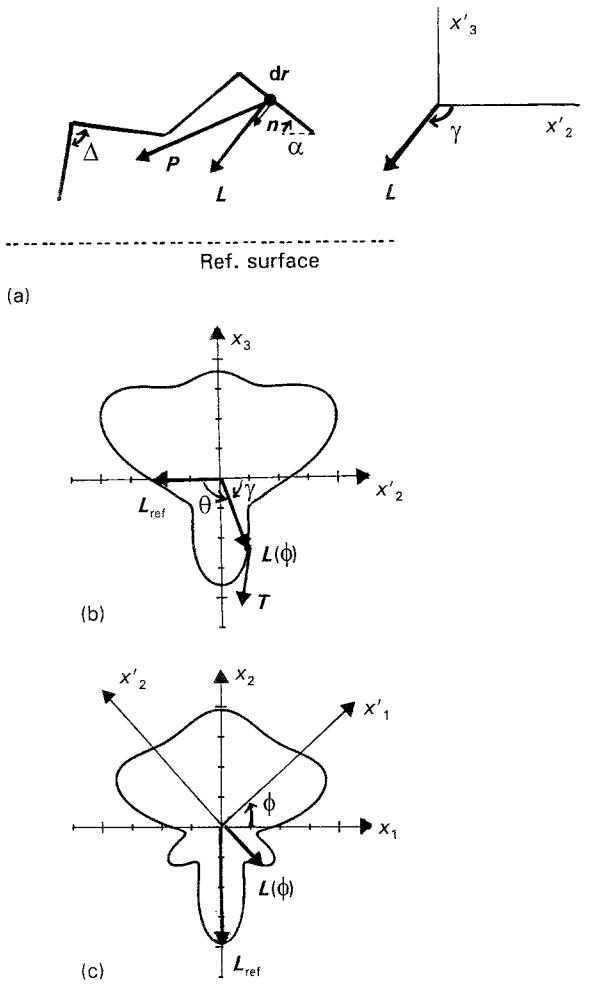

Figure 2 The two-dimensional model. (a) Representation of a surface profile. (b) Polar plot of $\boldsymbol{L}$ in a $(k\,h\,0)$ plane with $\boldsymbol{L}_{ref} = \boldsymbol{L}(\varphi = \varphi_0, \theta = 0°)$. Note that in the present work, owing to the symmetry properties of class $m\,3\,m$, we can start with a polar plot lying either in an $(\bar{h}\,k\,0)$ plane or in a $(k\,h\,0)$ plane. (c) Polar plot of $\boldsymbol{L}$ in a (0 0 1) plane. $\boldsymbol{L}_{ref}$ corresponds to $\boldsymbol{L}$ $(\varphi = 0°, \theta_0 = 0°)$.

D_{ij}, D_{ijk}, etc., of dissolution tensors [16, 17]. The number of dissolution constants is reduced by the symmetry the crystal class possesses and, as a result, the final equation (Equation 1 in Part I, [19]) is expressed in terms of angles of cut, φ and θ. Provided that the dissolution slowness depends only on the local orientation (φ, θ), of surface element, Tellier [17] has shown that a moving surface element, **d***s*, propagates along a straight line. Thus to each surface element we can associate a propagation vector, $\boldsymbol{P}$, which corresponds to the displacement of **d***s* within the crystal during an etching stage of duration dt (Fig. 1a).

We can also deal (Fig. 1b) with a polar representation, $L(\delta, \beta)$ of $\boldsymbol{L}$. In this case the two derivatives of $\boldsymbol{L}$ with respect to the polar angles (δ, β), define a plane, $\mathcal{P}$, tangent to the dissolution slowness surface at the point A of corresponding orientation. Geometrical considerations [17] give evidence that the propagation vector, $\boldsymbol{P}$, lies parallel to the normal, $\boldsymbol{N}$, to plane $\mathcal{P}$ (Fig. 1b). Because the polar angles are related to the angles of cut by means of the equations

$$\delta = \varphi + \frac{3\pi}{2} \tag{1a}$$

$$\beta = \theta + \frac{\pi}{2} \tag{1b}$$

the cartesian components of $\boldsymbol{P}$ can be calculated from the equation $L(\varphi, \theta)$, of the dissolution slowness.

In a two-dimensional kinematic model, a surface element, **d***s*, is replaced by a profile element, **d***r*, and thus we deal with the polar plot, lying in a starting cross-sectional plane (x'_2, x'_3). It is obvious that the propagation vector $\boldsymbol{P}$ lies now in the (x'_2, x'_3) plane and is perpendicular to the vector T tangent to the polar diagram $L(\gamma)$ of $\boldsymbol{L}$ (Fig. 2b). If we consider [18] the vector $\boldsymbol{T}$ as the derivative of the rotating vector $\boldsymbol{L}$ we can express the cartesian components, dx'_2 and dx'_3, of $\boldsymbol{P}$ by

$$dx'_2 = \pm \frac{B(\gamma)}{[L(\gamma)]^2} dt$$

$$dx'_3 = -\frac{A(\gamma)}{B(\gamma)} dx'_2 \tag{2}$$

where $A(\gamma)$ and $B(\gamma)$ are the cartesian components of $\boldsymbol{T}$, respectively.

This two-dimensional description is sufficient when we are concerned with profilometry traces of cross-sectional shape of starting circular sections. Effectively, the numerical procedure consists of evaluating the various propagation vectors associated with all profile elements composing the starting surface profile [7].

In the present work we investigate theoretical etching shapes related to a starting $(\bar{h}\,k\,0)$ silicon plane $(\varphi = \varphi_0, \theta = 0°)$. Depending on the etching shape under consideration, the numerical simulation involves a polar diagram lying in a $(k\,h\,0)$ plane or in the (0 0 1) plane. Thus taking into account the symmetry

properties of class $m3m$ the polar angle, γ, is simply connected with the angle of cut, θ (Fig. 2b) or with the angle φ (Fig. 2c), respectively. As a consequence we start either with the equation $L(\varphi = \varphi_0, \theta)$ in which θ varies with the orientation, α, of starting surface profile elements or with the equation $L(\varphi, \theta = 0°)$.

2.2. Correlation between final etching shapes and polar diagrams of L

2.2.1. Dissolution criteria

The dissolution criteria stated by Batterman [13] and later by Irving [21] are often used to predict approximate etching shapes for cross-sectional profiles (starting circular sections [3, 4, 7–11]) or of profilometry traces [1, 21]. Let us consider the situation illustrated in Fig. 2a and consider two surface profile elements Δr_1 and Δr_2 (i.e. two planes $\mathscr{P}_1$ and $\mathscr{P}_2$) intersecting at an angle Δ. We can conveniently restate the stability criteria in terms of the dissolution slowness as follows: a concave intersection is stable (the angle Δ remains unchanged with etching) provided there is no element (i.e. no plane) between them with a higher dissolution slowness, and conversely, a convex intersection remains stable when there is no element between Δr_1 and Δr_2 with a lower dissolution slowness. Stable intersections are associated with converging trajectories.

Diverging trajectories correspond to converse situations. If we are concerned with an initial surface profile composed of elements slightly disoriented with respect to the reference surface it is obvious that diverging trajectories cause the formation of rounded regions in the etched surface profile which flattens with repeated etchings [8, 15, 21]. Turning our attention to the final cross-sectional etched shape related to a starting cylindrical crystal, the angle, α, increases from 0° to 360°. As a consequence, the dissolution profile may be composed of highly disoriented linear segments associated with rapidly diverging trajectories [4, 7, 8]. These limiting facets correspond to minima in $\boldsymbol{L}$ when we start with a cylindrical crystal or to maxima in $\boldsymbol{L}$ when we etch a cylindrical hollow.

2.2.2. Rapid prediction of dissolution shapes

The dissolution criteria allow us to derive rapidly approximate two-dimensional dissolution shapes. Here we have to distinguish between cross-sectional profiles and surface profiles.

2.2.2.1. Cross-sectional profiles. Let us consider, for example, the case of a starting cylindrical crystal. The limiting shape must be connected with minima in the corresponding polar diagram for $\boldsymbol{L}$. It is evident that as $\boldsymbol{L}$ passes through an extremum the propagation vector $\boldsymbol{P}$ lies parallel to $\boldsymbol{L}$. Thus it becomes easy to construct geometrically an approximate limiting shape incorporating only linear facets associated with minima.

In reality, numerical simulation of cross-sectional profiles [7, 8, 11] has shown that etched profiles exhibit generally rather complex shapes. They are composed of successive planar and somewhat rounded regions where quasi-planar facets are correlated to accentuated minima in $\boldsymbol{L}$ whereas less pronounced secondary minima cause the formation of rather rounded facets. Moreover, the shape of dissolution cross-sectional profiles changes with the duration of etching because with repeated etchings the planar facets grow at the expense of the rounded regions.

2.2.2.2. Profilometry traces. Let the angle, α, of a starting profile element, Δr, be in the range between $-\alpha_{min}$ and $+\alpha_{max}$, that is to say, that in the case illustrated in Fig. 2b the angle θ covers a sector from $-\theta_{min}$ to $+\theta_{max}$ on the polar diagram of $\boldsymbol{L}$. In the case of profilometry traces we work simultaneously with concave and convex intersections so that the final dissolution shape depends on the complexity of the portion of the polar graph into consideration here, i.e. to the nature and to the number of extrema for $\boldsymbol{L}$ lying in the sector $(-\theta_{min}, +\theta_{max})$. In practice, we can distinguish between three characteristic situations illustrated in Table I where, for convenience, we have drawn the orientation dependence of $L(\varphi_0, \theta)$ in the form L versus α. These three interesting types of behaviour can be summarized as follows.

(i) When α varies in the range $(-\alpha_{min}, +\alpha_{max})$, $L(\alpha)$ passes through a single extremum which occurs for an orientation, $\alpha = 0°$, corresponding to the reference surface. As a consequence, a concave (or a convex) background develops if the extremum is a maximum (or a minimum) according to Irving's prediction [21]. The etched surface profile is thus essentially determined by diverging trajectories.

(ii) Suppose that in the range $(-\alpha_{min}, +\alpha_{max})$ we are now concerned with two successive extrema occurring at α_1 and α_2. The profile elements potentially present in the vicinity of α_1 and α_2 participate to the development of curved regions. As a result, the etched surface profile exhibits an alternate concave–convex (maximum of L for α_1, minimum for α_2) or convex–concave shape. However, in this case, care must be taken that the less accentuated are the two extrema, the more the alternate shape is easy to distinguish [8].

(iii) If three extrema for $\boldsymbol{L}$ are present in the investigated α-range, a complex and continuously evolving behaviour can result from repeated etching depending on the relative amplitude of successive extrema. However, the situations illustrated in column 3 of Table I merit some comments. Consider the first case presented in column 3: elements in the vicinity of α_{m1} and α_{m2} diverge markedly and thus form rapidly a profile composed of elements whose slopes close to α_{m1} and α_{m2} remain unchanged with prolonged etching. In addition, a formation of a rounded concave intersection associated with the maximum $L(\alpha_M = 0°)$ can come in the final stages of etching. Column 3 presents also the converse situation, with potentially an early development of a convex intersection around $\alpha_m = 0°$.

TABLE I Correlation between the etched shape of surface profiles and the nature and the number of extrema in the L versus α plot

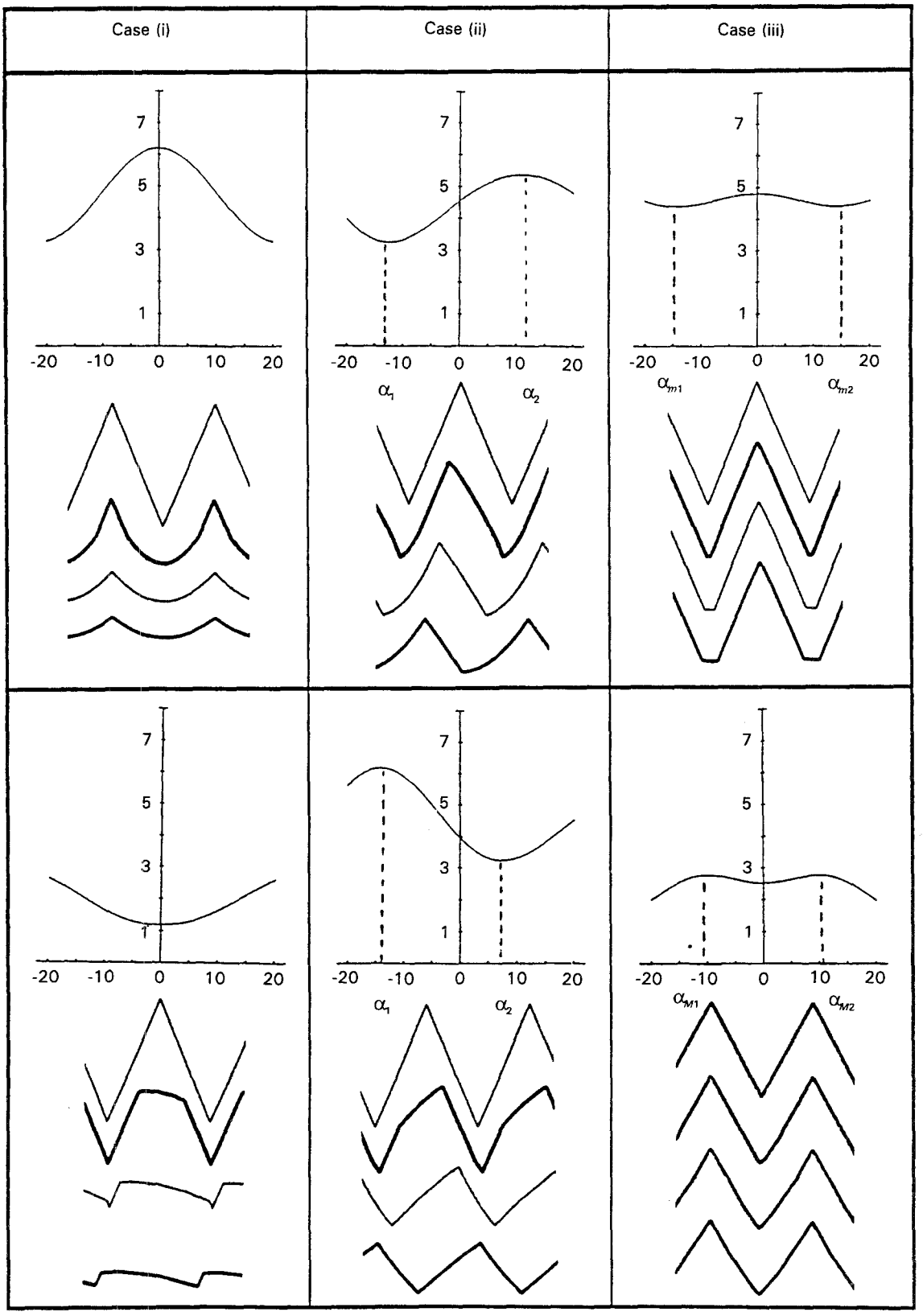

In reality, if trajectories associated with elements in the vicinity of α_{M1} and α_{M2} diverge rapidly (very accentuated maxima) the formation of the convex intersection is masked and only elements with slopes α_{M1} and α_{M2} contribute apparently to the etched surface profile.

From cases (ii) and (iii) described above, it appears that the geometrical features of profilometry traces can be modified by repeated etchings and that it remains very difficult to construct geometrically the etching shape of surface profiles. Only a numerical simulation based on the tensorial model for chemical etching allows us to derive the exact etching shape and to outline the important role played by the relative amplitude of successive extrema in L.

However, let us remark that in Part I [19] we have partly made use of features described in Table I to derive the dissolution slowness surface of a silicon

crystal. This is the reason why it is necessary to verify the adequation of the proposed slowness surface by means of a numerical simulation.

3. Numerical simulation of two-dimensional dissolution shapes

As noticed in Section 2, experimental results are related to $(\bar{h}\,k\,0)$ silicon planes, and the numerical simulations start with polar diagrams in the form $L(\varphi = \varphi_0 + 90°, \theta)$ or $L(\varphi, \theta_0 = 0°)$, i.e. for a crystal belonging to class $m\,3\,m$ with diagrams lying in an $(\bar{h}\,k\,0)$ or a (0 0 1) plane, respectively. The simulation programs have been described elsewhere [7, 22]. Here it is sufficient to know that in the first step we work with all the potentially present elements of the starting profile and that in the last step tests are made to distinguish between diverging and converging trajectories and to eliminate at each etching stage the elements which do not contribute to the etched profile.

To establish easily correlations between the proposed shape for the dissolution slowness surface and the final shape for dissolution profiles, we present, in addition, the polar diagrams of $\boldsymbol{L}$ corresponding to $(\bar{h}\,k\,0)$ sections (simulation of etching shapes for initially circular sections) and the part of L versus α plots involved in the theoretical prediction of etched surface profiles.

3.1. Numerical simulation of cross-sectional profiles

The $(\bar{4}\,1\,0)$ cross-section of a silicon cylindrical crystal etched in an aqueous KOH solution exhibits a relatively complex shape [19] characterized by the presence of three different minima and three different maxima in the out-of-roundness profiles. This is the reason why we have generated a dissolution slowness surface by evaluating dissolution constants related to a tensor of rank $N_{max} = 18$. As a result we obtain the polar diagrams. $L(\varphi = \varphi_0, \theta)$, displayed in Fig. 3 and lying in various $(k\,h\,0)$ planes.

In the case of initially cylindrical crystal or thick circular plates the potentially present profile elements lie in an $(\bar{h}\,k\,0)$ plane and correspond to traces of planes tangent to the starting circular section at points defined by the angle $\varphi = \varphi_0 + 90°$ and the varying angle θ. Taking into account the point group symmetry 4 about the [0 0 1] axis, we thus make use of $(k\,h\,0)$ polar diagrams illustrated in Fig. 3 to predict the theoretical shape of etched thick circular plates (Fig. 4). In addition, the corresponding out-of-roundness is superimposed to the etched section. The program gives also the theoretical angular positions (Table II) of maxima and minima in the various out-of-roundness profiles.

A complete examination of Figs 3 and 4 and of Table II reveals several interesting features.

1. As mentioned in Part I [19], an out-of-roundness profile constitutes an approximate "image" of the corresponding polar diagram. This observation justifies the procedure we have chosen in Part I to generate the dissolution slowness surface.

TABLE II Angular positions of peaks (θ_M) and valleys (θ_m) appearing in the theoretical out-of-roundness profiles related to various $(\bar{h}\,k\,0)$ sections (angle of cut φ_0)

φ_0 (deg)	Etchant "KOH", rank 18	
	Maxima θ_M (°)	Minima θ_m (°)
0	0, 45, 90	26, 64
5	0, 55, 90	35, 63
10	3, 41, 90	0, 41
14	10, 37, 90	0, 29, 50
18	10, 38, 90	0, 22, 55
23	8, 37, 90	0, 16, 59
26	4, 37, 90	0, 13, 60
30	0, 36, 90	11, 61
34	0, 36, 90	9, 62
37	0, 36, 90	9, 62
42	0, 35, 90	8, 62
45	0, 35, 90	8, 63

2. In the framework of dissolution criteria the minima appearing in out-of-roundness profiles related to convex sections are correlated to the development of quasi-planar facets connected with minima in $\boldsymbol{L}$. As a consequence, angular positions of valleys in the theoretical and experimental out-of-roundness profiles must coincide. Table III indicates that for φ_0 in the range [0°, 18°] we obtain reasonable departures between theoretical and experimental values. As φ_0 reaches 23° (Fig. 3) the theoretical minimum is displaced toward $\theta_m \approx 10°$ whereas a maximum in $\boldsymbol{L}$ takes place at $\theta_M \approx 0°$. Thus one can reasonably expect to observe a peak and a valley at similar positions in the corresponding experimental out-of-roundness profile ([19], Fig. 15f). Thus at the first sight, Tables II and III reveal an apparent disagreement between theory and experiment. But care must be taken that L passes rapidly from a maximum at $\theta_M \approx 0°$ to two accentuated minima located at $\theta_{m1} = -9°$ and $\theta_{m2} = 9°$, respectively. In the vicinity of these two minima, the trajectories of profile elements diverge markedly. As a result, the extent of the rounded portion associated with L_{max} ($\theta = 0°$) is seriously masked by the development of the planar facets correlated with the two minima in $\boldsymbol{L}$. Thus it can become difficult to detect the presence of such a maximum in the experimental out-of-roundness profiles.

3. For φ_0 in the range (0°, 18°) the theoretical shape of out-of-roundness profiles changes continuously with φ_0. The more rapid change occurs for φ_0 close to 14°. This observation agrees well with experimental results (Fig. 15a–e in [19]).

4. As φ_0 increases 26° to 45°, both the experimental and theoretical out-of-roundness profiles show quite similar geometrical features. All the profiles are characterized by the presence of a large maximum located at $\theta \approx 36°$ (see, for example, Tables II and III). This maximum is correlated to a $\{1\,1\,1\}$ plane which etches very slowly [1, 23–26].

5. The fact that, in theory and in experiments ([19] Table III), angular positions, θ_M, of peaks in the out-of-roundness profiles remain quasi-insensitive to the duration, t, of etching, and coincide exactly with the angular positions of maxima in the corresponding

polar diagram of $\boldsymbol{L}$ may be attributed to the high degree of symmetry of the class $m\,3\,m$. Effectively, it has been shown [8] that, in general, the shape of dissolution profiles changes with repeated etchings, because the limiting planar facets grow at the expense of curved regions. As a consequence, positions θ_M depend on the etching time, t. In contrast, quite symmetrical portions of a polar diagram leave the angular positions, θ_M, unchanged on prolonged etching. This is just the situation revealed by polar graphs displayed in Fig. 3.

From the preceding remarks, we can infer that the numerical simulation remains in fair agreement with experiments. We have just to justify the possible presence of a maximum in $L(\varphi_0, \theta)$ for θ around 0° when the angle of cut, φ_0, lies in the range [26°, 45°].

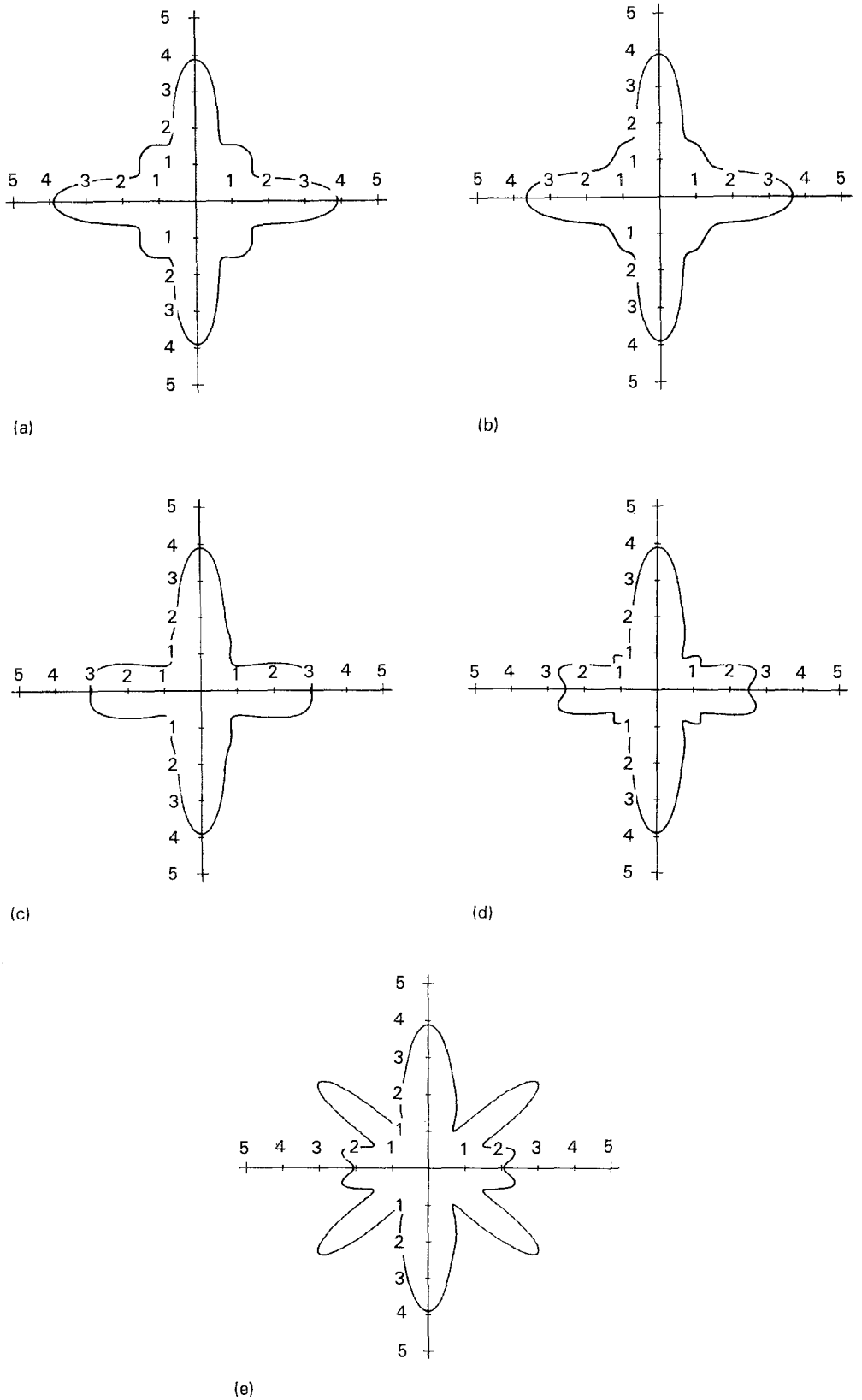

Figure 3 Polar plots of $\boldsymbol{L}$ in various ($k\,h\,0$) sections in KOH 18. (a–j) are for sections corresponding to $\varphi_0 = 0°, 5°, 10°, 14°, 18°, 23°, 26°, 30°, 34°$, and 45°, respectively. As $L(\varphi_0, \theta)$ takes large values for $\varphi_0 \geqslant 23°$, the polar plots represent ln $[L(\varphi_0, \theta)]$ for φ_0 in the range [23°, 45°].

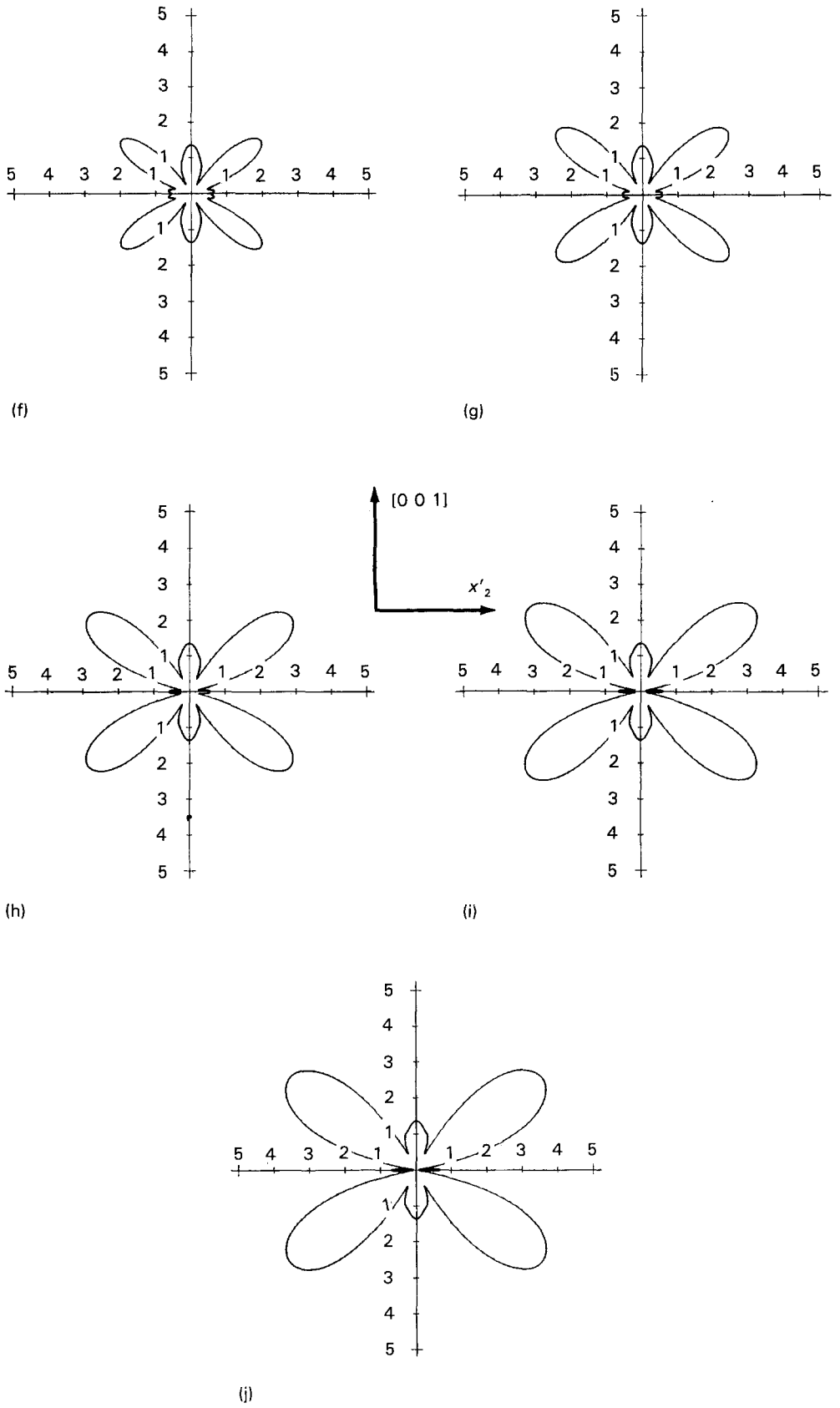

Figure 3 (*Continued*).

Moreover care must be taken because we cannot determine precisely the accentuation of the various extrema in $\boldsymbol{L}$ from a direct comparison of experimental and theoretical out-of-roundness profiles. Fortunately, to discuss the adequation of the proposed slowness surface, we can also derive theoretical profilometry traces related to starting rough surfaces [8, 9, 15, 22]. Such a numerical simulation can give us additional interesting informations on the real angular positions of extrema in $\boldsymbol{L}$ as well as on the relative amplitude of successive extrema.

3.2. Numerical simulation of profilometry traces

In this section some attempts are made to establish the

adequation of the dissolution slowness surface proposed in Part I by predicting shapes of x_1' (or x') and [0 0 1] profilometry traces. For simplicity, as a first step, we work with initially triangular profiles whose convex and concave intersections are formed by linear elements with slopes equal to $\pm \alpha_{max}$. In the second step, we start with a "real" surface profile as given by a microprocessor-based surface profilometer. In this last case, theoretical traces are then numerically worked at various etching times in order to extract complementary information from the successive distributions of slopes [27].

As noticed earlier, we have chosen in these two steps to investigate the changes with orientation, φ_0, in the etching shape of traces made along the rotated x_1' axis and along the [0 0 1] axis. Let the initial distribution of slopes extend from $-\alpha_{min}$ to α_{max}. The profile elements composing the initial x_1' trace lie in the (0 0 1) plane. Thus in the numerical simulation, we use a portion $(-\alpha_{min}, +\alpha_{max})$ of the (0 0 1) polar plot centred on $L(\varphi = \varphi_0, \theta = 0°)$. The profile elements of a [0 0 1] profilometry trace made on an $(\bar{h}\,k\,0)$ plate (angle of cut φ_0) are located in the plane $(k\,h\,0)$. We thus work with the polar diagram corresponding to an

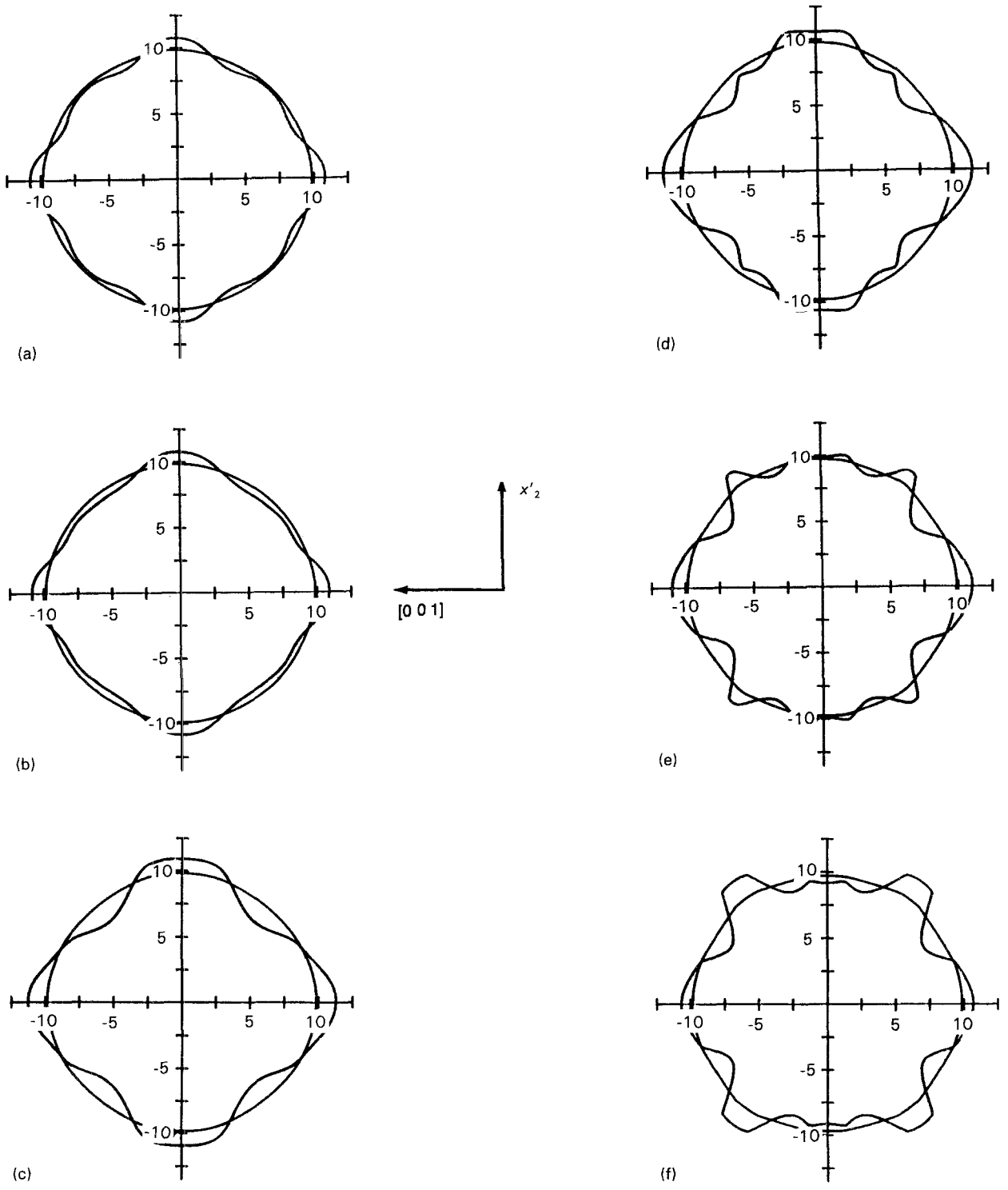

Figure 4 Theoretical etched shapes for $(\bar{h}\,k\,0)$ initially circular sections and the corresponding out-of-roundness profiles. (a–l) are for sections corresponding to $\varphi_0 = 0°$, 5°, 10°, 14°, 18°, 23°, 30°, 34°, 37°, 42° and 45°, respectively. $N_{max} = 18$, KOHF–NR18, $\varphi = 0$.

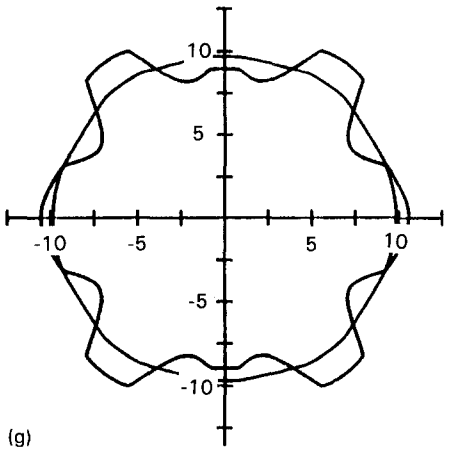

(g)

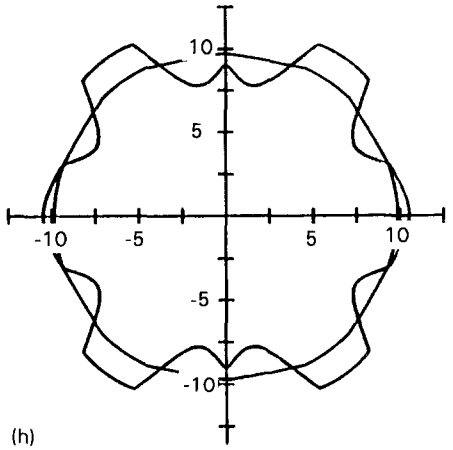

(h)

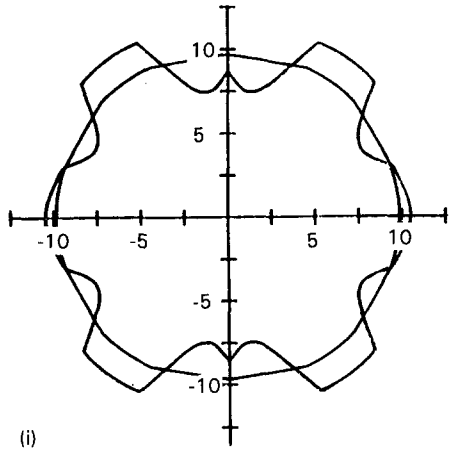

(i)

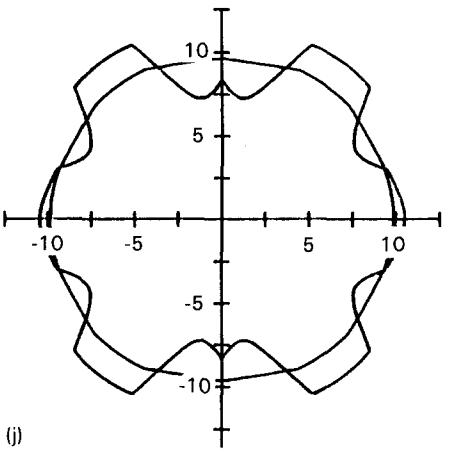

(j)

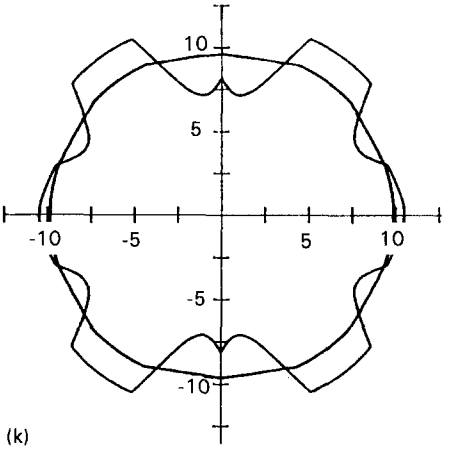

(k)

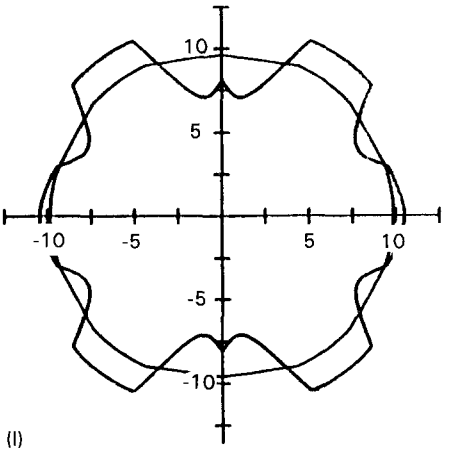

(l)

Figure 4 (*Continued*).

angle of cut $\varphi = \varphi_0 + 90°$. Taking into account the four-fold symmetry about the [0 0 1] axis which the class $m3m$ possesses, it is obvious that we obtain identical shapes for [0 0 1] traces by simply starting with the portion of the $(\bar{h}k0)$ polar graph where the dissolution slowness related to the reference surface lies evidently parallel to the rotated axis.

3.2.1. Theoretical shape of etched triangular surface profiles

For a starting triangular profile with slopes $\alpha_{min} = \alpha_{max} = 15°$ the numerical simulation provides for various etching times, t, the successive surface profiles displayed in Figs 5 and 6. In addition, Figs 5 and 6 show also the corresponding L versus α plots. This type of simulation appears as very convenient when we search to establish rapidly a correlation between the presence of extrema in L versus α plots and the etching shape of profiles.

In particular from Figs 5 and 6 we collate several pieces of information in close agreement with predictions (see Table I) deduced from the dissolution criteria.

1. When the L versus α plot presents a single extremum for an orientation $\alpha = 0°$ we obtain effectively a convex or a concave background (Fig. 5a, d,f). An accentuated or "sharp" extremum causes the rapid formation of a rounded background, together with an early flattening of the trace (compare Fig. 5a and f, for example).

2. A profilometry trace with an alternate shape results from the existence of two extrema for $L(\alpha)$ in the range $[-\alpha_{min}, +\alpha_{max}]$ (Fig. 5b, c, e).

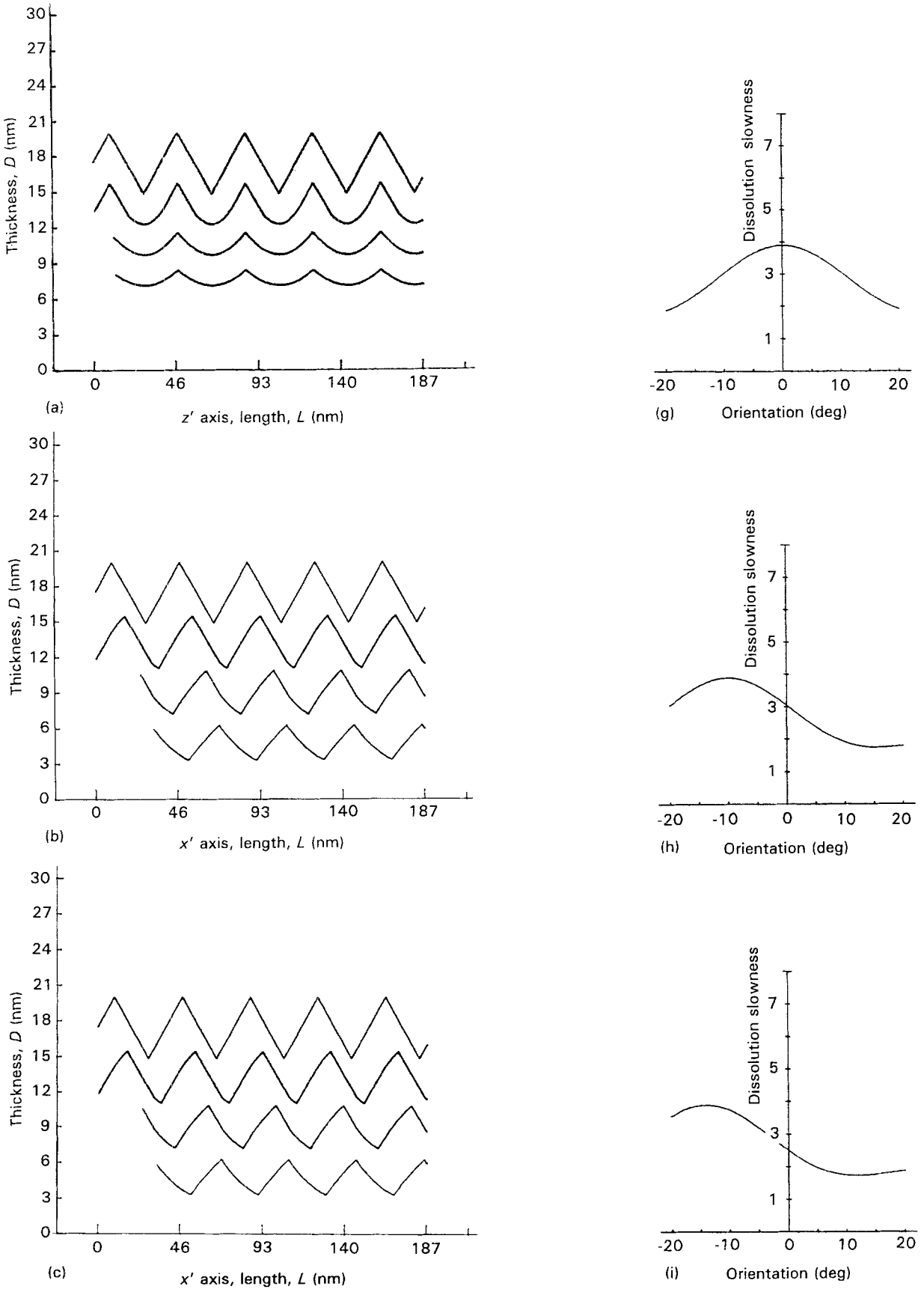

Figure 5 Successive theoretical etched shapes for x'_1 traces as derived from the corresponding $L(\alpha)$ versus α plots. The duration of etching is successively equal to $t = 10$, 20 and 30 arb. units. The angle φ_0, of cut for the various planes is respectively: (a, g) $\varphi_0 = 0°$; (b, h) $\varphi_0 = 10°$; (c, i) $\varphi_0 = 14°$; (d, j) $\varphi_0 = 23°$; (e, k) $\varphi_0 = 34°$; (f, l) $\varphi_0 = 45°$.

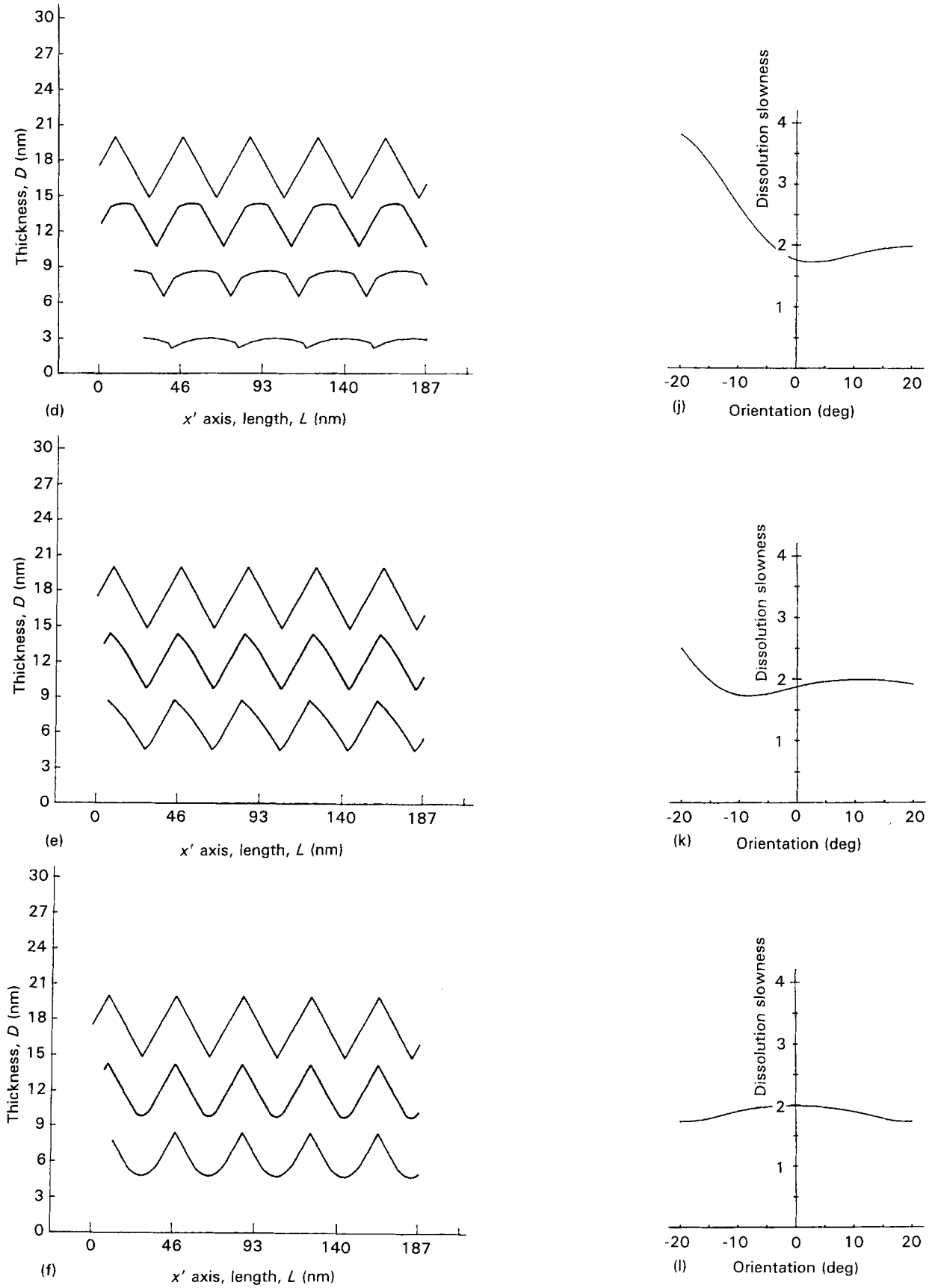

Figure 5 (*Continued*).

3. Consider now the cases where L passes through three extrema (Fig. 6h–l). Profiles with constant slopes form rapidly if two rather sharp minima in $\boldsymbol{L}$ lie symmetrically to a maximum (Fig. 6k, l). The concave intersections tend to be rounded with further etchings. The converse situation (two maxima and a minimum in $\alpha = 0°$) gives also a profile (Fig. 6b–d) whose slopes are quasi-unmodified with prolonged etching. Because in the α range investigated here we only observe slight variations in L the formation of rounded intersections associated with the minimum in L remains ineffective with prolonged etching.

3.2.2. Theoretical shape of etched "real" surface profiles

A profilometry trace was made on a lapped surface so that the initial profile (Fig. 7) has slopes extending from $-59°$–$24°$. However, the major part of profile elements possesses a slope lying in the range $(-27°, 24°)$ (Fig. 7b). As the L versus α plot can exhibit several extrema in the total α range investigated here, the

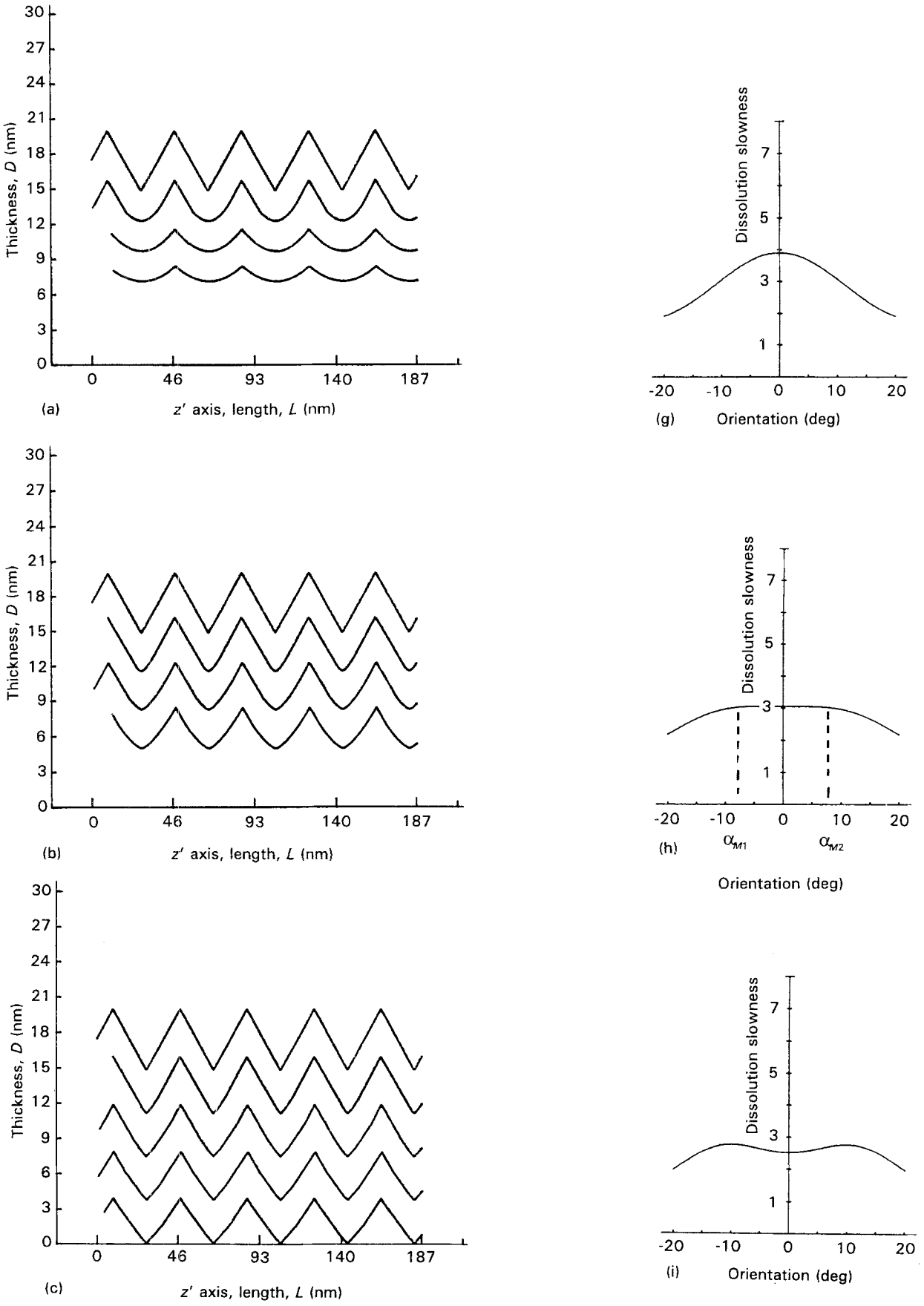

Figure 6 Successive theoretical etched shapes for [0 0 1] traces as derived from the corresponding $L(\alpha)$ versus α plots. The duration of etching is successively equal to $t = 10, 20, 30$ and 40 arb. units. The angle, φ_0, of cut for the various planes is respectively: (a, g) $\varphi_0 = 0°$; (b, h) $\varphi_0 = 10°$; (c, i) $\varphi_0 = 14°$; (d, j) $\varphi_0 = 23°$; (e, k) $\varphi_0 = 34°$; (f, l) $\varphi_0 = 45°$.

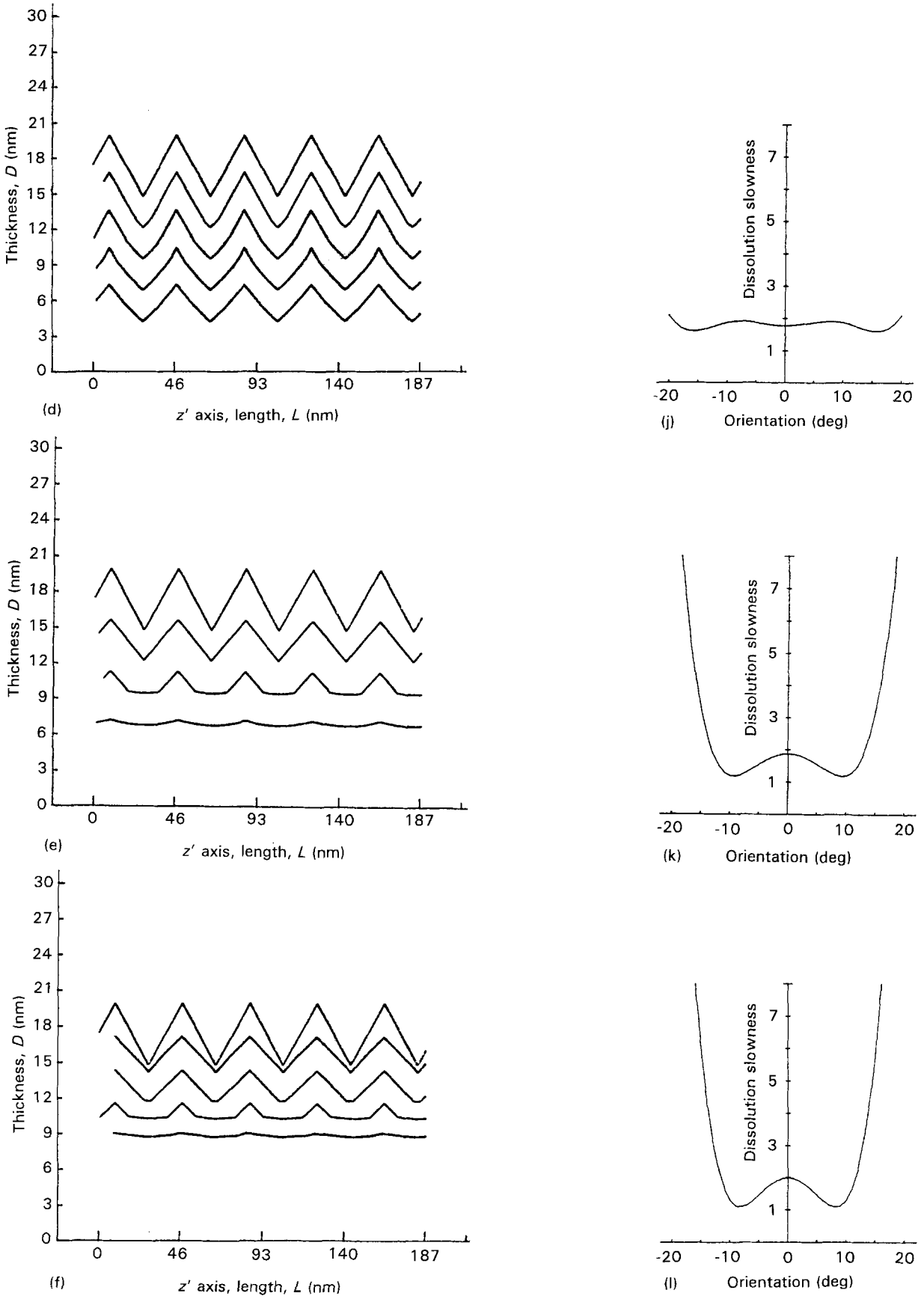

Figure 6 (*Continued*).

theoretical dissolution profile can, consequently, present complex geometrical features.

The simulation program furnishes digitalized profilometry traces which can be treated separately [27] to visualize total surface profiles (see Fig. 8a–c, for example) and corresponding distributions of slopes (Fig. 8d–f, for example). In this condition it may be interesting to follow changes in theoretical shapes of

TABLE III Final (t = 45 min) angular positions for the successive extrema in the various experimental out-of-roundness profiles relative to differently oriented silicon plates (angle of cut φ_0)

φ_0 (deg)	0	5	10	14	18	23	26	30	34	37	42	45
Maxima θ_e (deg)	0, 45, 90	0, 45, 90	0?, 45, 90	10, 43, 90	12, 41, 90	40, 90	36, 90	37, 90	37, 90	34, 90	35, 90	36, 90
Minima θ_e (deg)	27, 63	28, 62	28, 64	0, 27, 63	0, 23, 62	0, 63	0, 63	0, 64	0, 63	0, 61	0, 62	0, 64

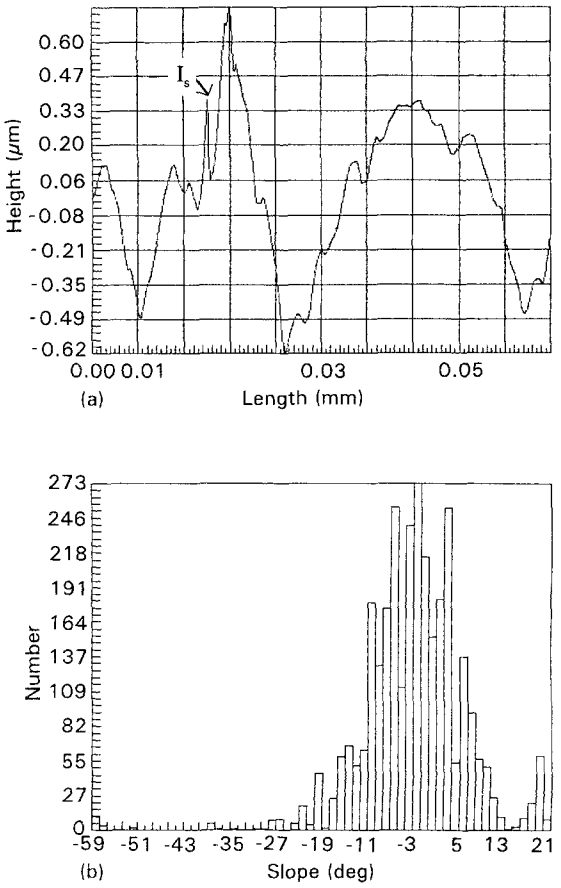

Figure 7 Experimental profilometry trace characteristic of a rough surface: (a) surface profile; (b) corresponding distribution of slopes.

traces (Figs 8a–c–12a–c) and in corresponding distributions of slopes (Figs 8d–f–12d–f) with the etching time, t.

Let us first examine the various theoretical [0 0 1] traces. For the cut $\varphi_0 = 10°$ (Fig. 8), concave and convex regions are simultaneously present in theoretical traces. It is clear that concave regions are connected with the two maxima which occurs for α_{M1} and α_{M2}, whereas convex parts are associated with the minimum in L at $\alpha = 0°$ (Fig. 6h). Only elements with large slope ($|\alpha| > 15°$) which etch rapidly disappear rapidly (see Fig. 8d and e) whereas elements in the range $[-15°, +15°]$ contribute longer to the etched profile. Then the etched profile possesses a weakly evolving distribution of slopes in relative agreement with experimental observation (Fig. 5 of Part I). Consider now the theoretical [0 0 1] trace related to a [1 1 0] plate (Fig. 9). The successive distributions of slopes give evidence for the existence of two minima in L lying symmetrically with respect to the maximum located at $\alpha = 0°$. The theoretical traces show regions characterized by constant slopes ($\pm \alpha_m$ with $\alpha_m \approx 9°$) and concave regions with slightly disoriented elements. Moreover, care must be taken because some profile elements have been omitted in the final trace (Fig. 9c). Effectively, when we work with very rough surfaces the increment, $\Delta\alpha$, in α involved in simulation can approach 6° for some sharp intersections (as intersection l_s in Fig. 7a). Then the influence of some extrema can be partly masked resulting in the truncation of final traces. In reality, only Fig. 9a and b seem representative of the [0 0 1] etched profile. This explanation is sufficient to describe also the behaviour of the predicted [0 0 1] traces related to the cut $\varphi_0 = 34°$ (Fig. 10).

Turning our attention to the simulation of some x'_1 traces we observe the following points.

(i) A profile with alternate concave–convex shape (Fig. 11) results from the presence of two extrema in the L versus α plot. The corresponding asymmetric distribution of slopes splits into two distinct peaks as the etching time, t, increases (Fig. 11e). The extent of the peak associated with positive slopes is larger than that related to negative slopes because trajectories of elements with negative slope diverge more rapidly (the maximum in L is less accentuated than the minimum, Fig. 5k). The angular position of these two peaks remains crudely unchanged with repeated etching because the two extrema in L can be considered as "smooth" extrema. It has been effectively demonstrated [8] that only "sharp" extrema induce changes in the angular position of peaks with the duration of etching.

(ii) When a concave background (Fig. 12) develops according to the scheme described in Table I the profile flattens with prolonged etching. We obtain a somewhat symmetrical distribution of slopes where larger slopes disappear progressively.

3.2.3. Comparison with experiments and conclusion

To compare easily the theoretical shape of surface profiles with that of experimental traces, we have collected the final x'_1 and [0 0 1] theoretical traces in Figs 13 and 14, respectively. The comparison is based essentially on two points:

(i) the visual geometrical aspect of profiles with a classification in terms of fundamental shape (convex, concave, alternate, constant slopes...);

(ii) the features which characterize the final distribution of slopes (extend E, angular positions of peaks in particular).

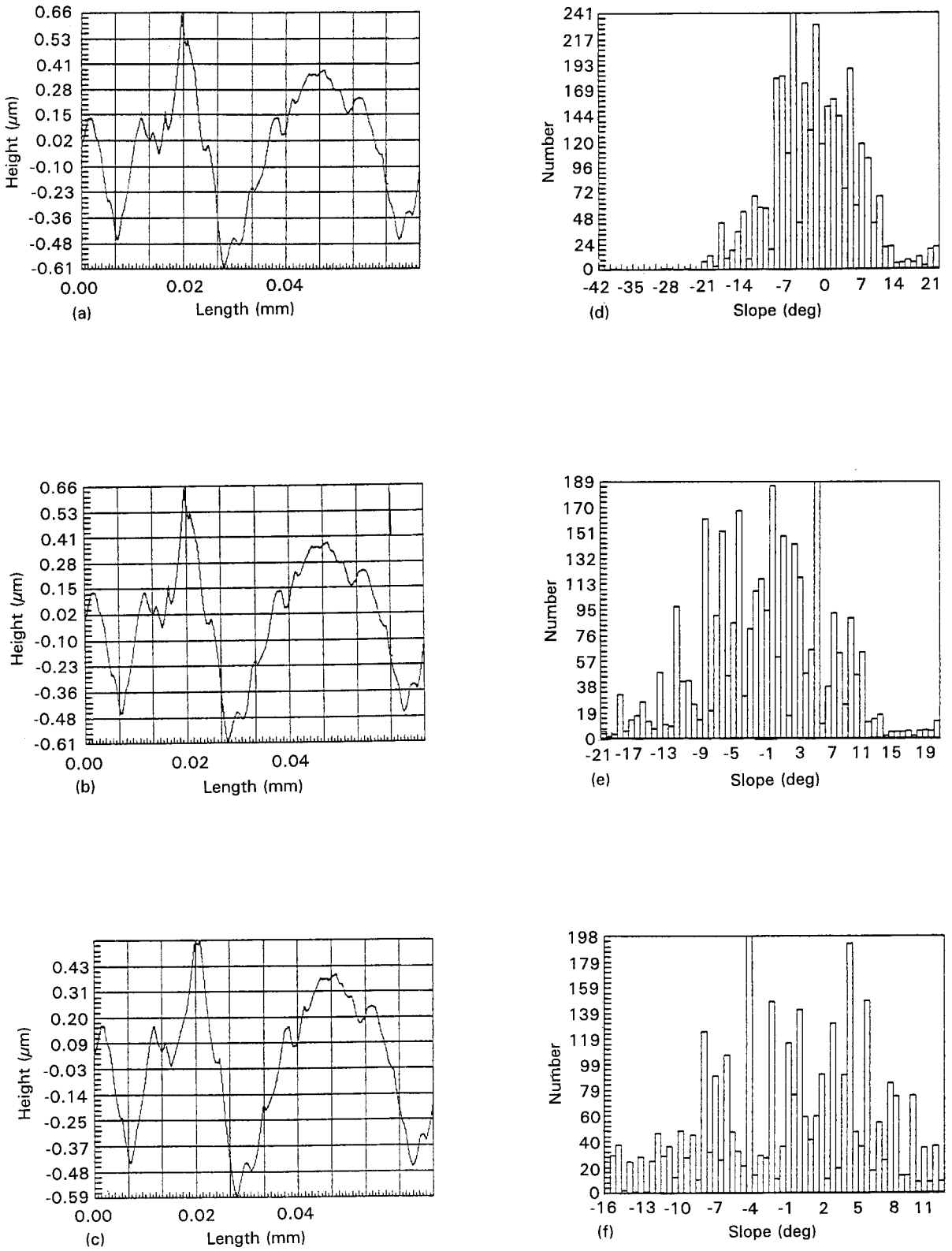

Figure 8 Theoretical changes in the etched shape of a "rough" surface profile and in the distribution of slopes with the duration of etching, t, for the case of a [0 0 1] trace made on a plane $\varphi_0 = 10°$. (a, d) $t = 0.5$ arb. units; (b, e) $t = 1$ arb. units; (c, f) $t = 3$ arb. units.

Taking into account that, from Section 3.2.2, we have to distinguish between two regions in profiles (i.e. elements with large slopes and elements with small slopes), Tables IV and V give the major features for theoretical x'_1 and [0 0 1] traces, respectively. As the initial distribution of slopes differs markedly from a Gaussian distribution, it is not easy to distinguish secondary peaks. Thus we have chosen, in the third column of Table IV, to indicate the angular position of the principal peak (P_1) only for which no doubt subsists. This difficulty arises for x'_1 traces essentially. For convenience the etching shape characterizing experimental x'_1 and [0 0 1] profilometry traces are summarized in Table VI. In addition, tentative attempts are made in Table VII to clarify the features of corresponding distributions of slopes. Here we discuss briefly the limitations imposed by the profiling instrumentation. It is well known [28] that a stylus (here a

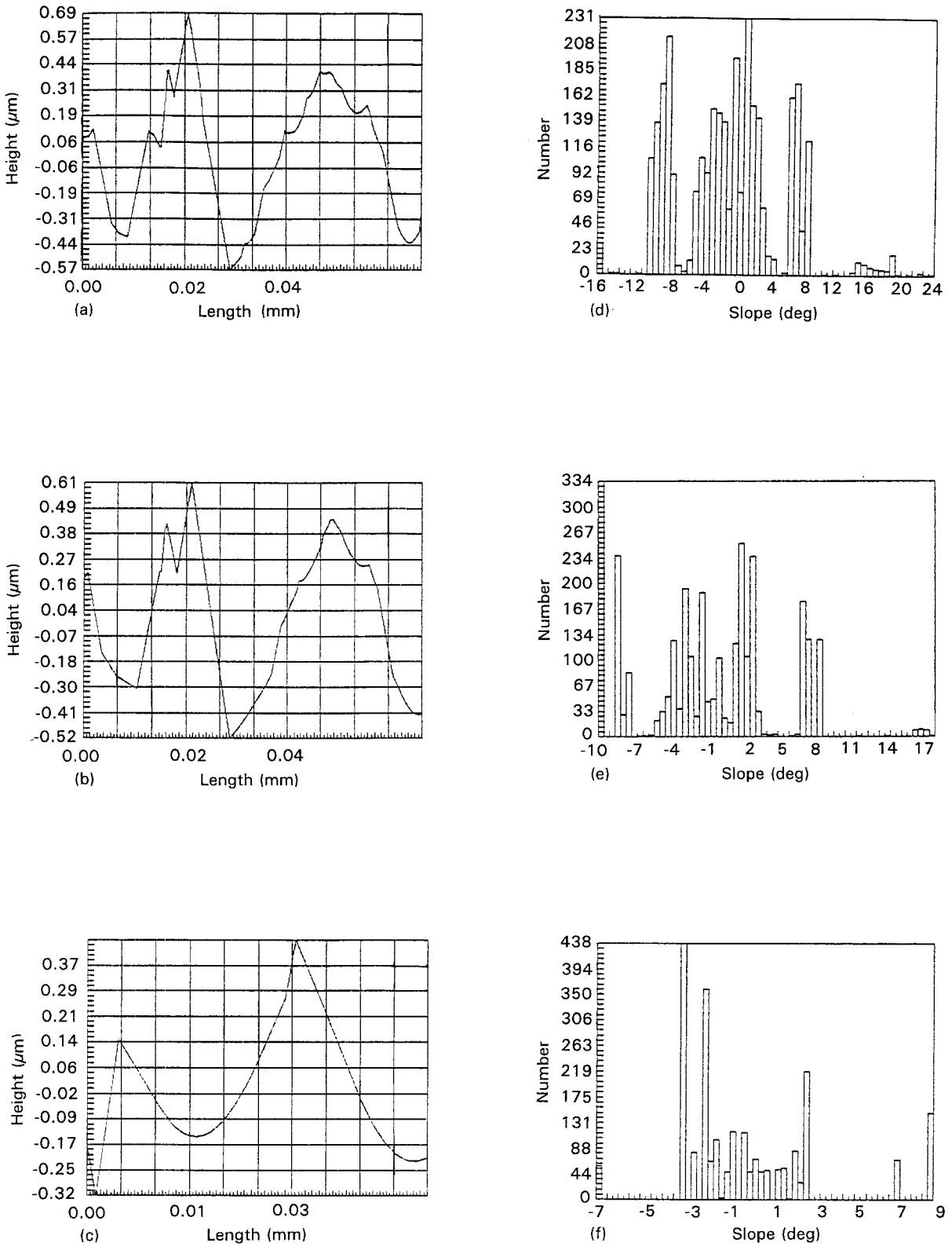

Figure 9 Theoretical changes in the etched shape of a "rough" surface profile and in the distribution of slopes with the duration of etching, t, for the case of a [0 0 1] trace made on a plane $\varphi_0 = 45°$. (a, d) $t = 0.5$ arb. units; (b, e) $t = 1$ arb. units; (c, f) $t = 3$ arb. units.

diamond tip of about 2.5 μm) of finite size moving on a rough surface provides a first "mechanical filtering" which results in an attenuation of the vertical amplitude of peaks. This "smoothing" effect is a source of error for the distribution of slopes.

Moreover, sharp peaks are rounded, whereas curved valleys appear as sharp concave intersections in profilometry traces. The mechanical filtering also affects the shape of traces; consequently, for etched surfaces with close asperities, the identification of the true "dissolution shape" can be a problem. In most cases, experimental distributions associated with convex or concave backgrounds appear more peaky at $\alpha = 0°$ relative to true distributions. Furthermore, because a surface profile of alternate shape is smoothed because of the finite tip which acts as a mechanical filter, we generally observe the persistence of a principal peak centred on $\alpha = 0°$ even if such a

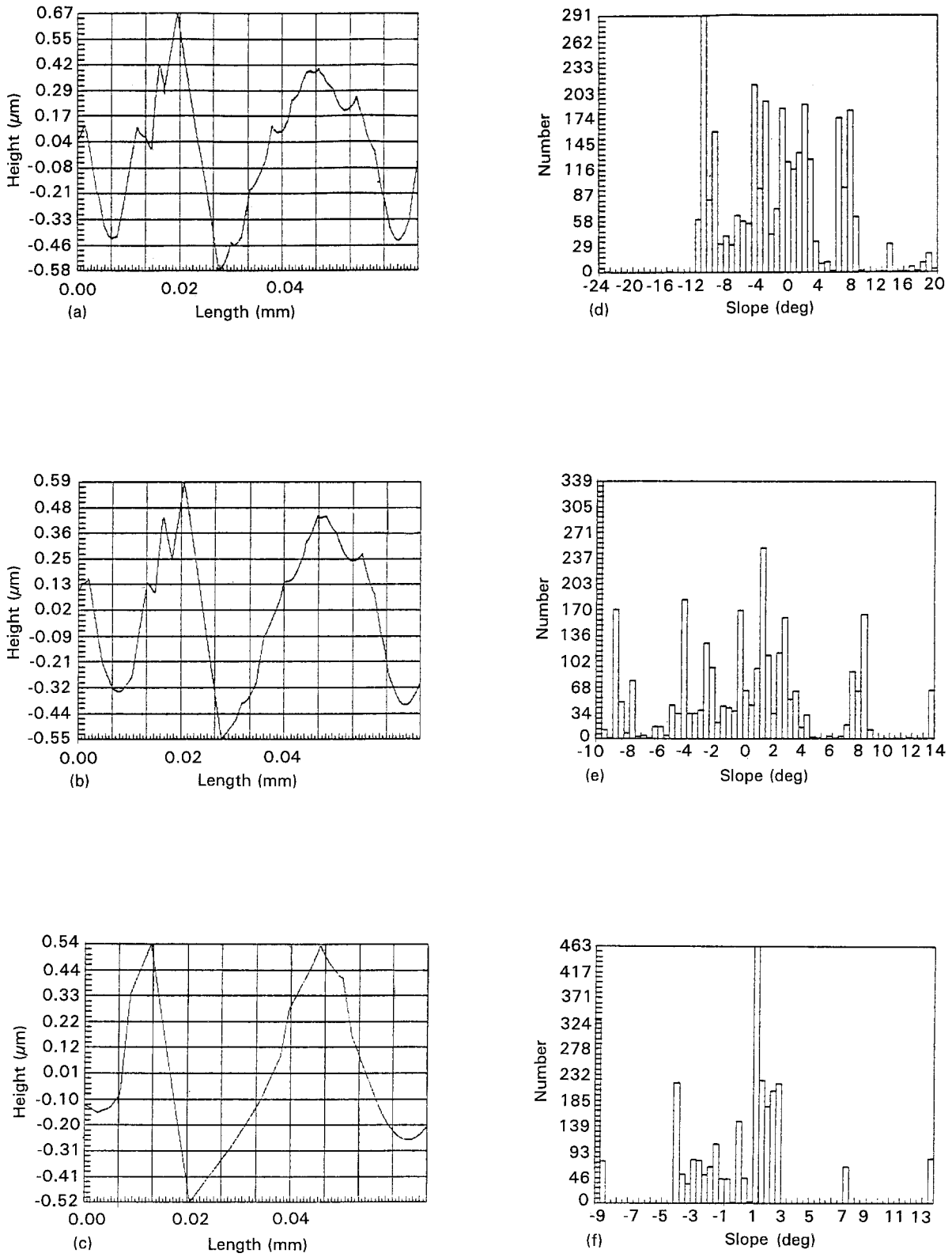

Figure 10 Theoretical changes in the etched shape of a "rough" surface profile and in the distribution of slopes with the duration of etching, t, for the case of a [0 0 1] trace made on a plane $\varphi_0 = 34°$. (a, d) $t = 0.5$ arb. units; (b, e) $t = 1$ arb. units; (c, f) $t = 3$ arb. units.

trace which presents sharp discontinuities at convex and concave intersections is, in theory, characterized by the absence of a central peak [8]. For these various reasons, care must be taken when tentative attempts are made to correlate experimental distributions of slopes with extrema in $\boldsymbol{L}$.

We now proceed to compare experimental and theoretical [0 0 1] traces. A fair agreement between experimental and theoretical traces is revealed by examination of Tables V, VI and VII. Moreover, for φ_0 within the range [30°, 45°], the experimental angular positions of the so-called secondary peaks (SP) coincide with those related to theoretical traces. As the angle φ_0 increases from 10° to 23° we do not observe in experiments all the theoretical peaks mentioned in the third column of Table V, but only a central peak

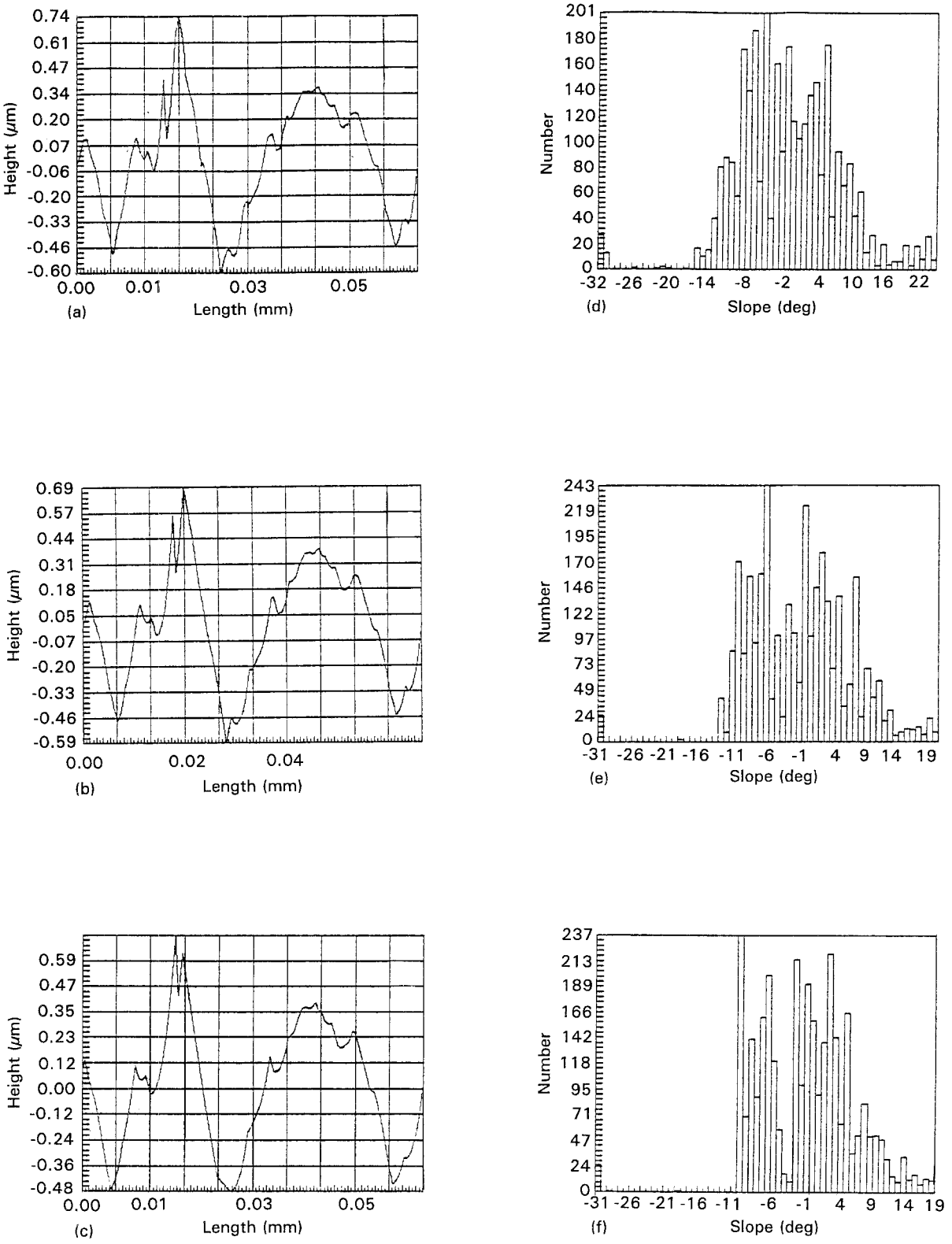

Figure 11 Theoretical changes in the etched shape of a "rough" surface profile and in the distribution of slopes with the duration of etching, t, for the case of a x'_1 trace made on a plane $\varphi_0 = 34°$. (a, d) $t = 1$ arb. units; (b, e) $t = 3$ arb. units; (c, f) $t = 5$ arb. units.

(CP at $\alpha = 0°$). However, there is no contradiction between theory and experiment because the experimental distribution covers a range $(-10°, +10°)$. Because the number of elements with slope in the vicinity of $-9°$ or $9°$ is very limited, it is not surprising that one cannot distinguish secondary peaks associated with extrema in $\boldsymbol{L}$ close to $\pm 9°$. Moreover for $\varphi_0 = 18°$, the experimental distribution appears relatively flat and broad. This is probably due to weak variations in L with α for φ_0 in the vicinity of 23° in accord with the theoretical L versus α plot displayed in Fig. 6d.

Let us now compare in Tables IV, VI and VII results related to x'_1 traces. Here, again, we observe a good agreement between theoretical and experimental shapes. The connection between experimental and theoretical distributions of slopes seems more difficult to establish (Tables IV and VII). Effectively, there is

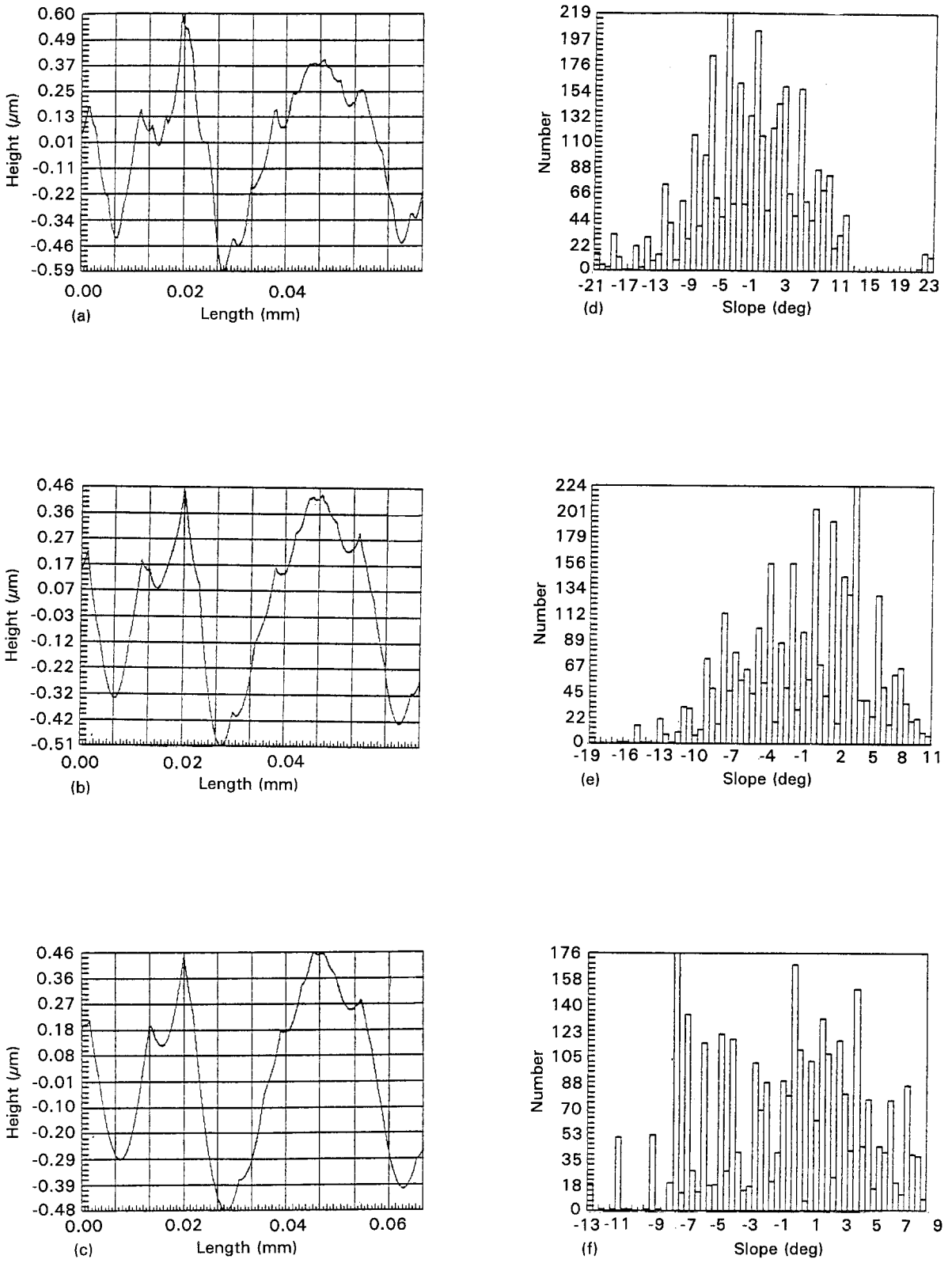

Figure 12 Theoretical changes in the etched shape of a "rough" surface profile and in the distribution of slopes with the duration of etching, t, for the case of a x_1 trace made on a plane $\varphi_0 = 0°$. (a, d) $t = 1$ arb. units; (b, e) $t = 3$ arb. units; (c, f) $t = 5$ arb. units.

sometimes a weak difference between heights of the two peaks (denoted P_1, P_2) which occur in the distribution of slopes related to experimental or theoretical traces with alternate shape [8].

Therefore, the distinction between secondary peak (SP) and principal peak (PP) which can appear as tendentious, is not used in Table IV. In addition, in some theoretical traces, only the angular position of one of the two peaks can be determined with a sufficient accuracy. However, despite these difficulties, Tables IV and VII show that, in most cases, angular positions of peaks P_1 or P_2 (Table IV) deviate from those of peaks called "SP" and "PP" (Table VII) by less than 3°. Only the cut $\varphi_0 = 34°$ does not follow this description but, in this case, a flat and broad peak is observed in the theoretical distribution.

A careful examination of Tables IV–VII reveals a close agreement between theory and experiments. We

can thus infer that the theoretical shape for the dissolution slowness surface, proposed in Part I is not far from the true shape, even if the true amplitude of extrema in $\boldsymbol{L}$ cannot be easily estimated from the present comparison. In particular it is clear that the slowness surface presents minima minimora for orientations ($\varphi_0 = 45°$, $\theta \approx \pm 9°$) and related orientations. The development of a [0 0 1] surface profile characterized by constant slopes ($\alpha \pm 9°$) is undoubtedly due to these minima. The maximum in $\boldsymbol{L}$ located at ($\varphi_0 = 45°$, $\theta = 0°$) must, in addition, cause the formation of rounded concave intersections which in [0 0 1] experimental profilometry traces are masked by the so-called "mechanical filtering". Turning to Fig. 15, which shows the corresponding [0 0 1] surface profile restored by picture processing of an atomic

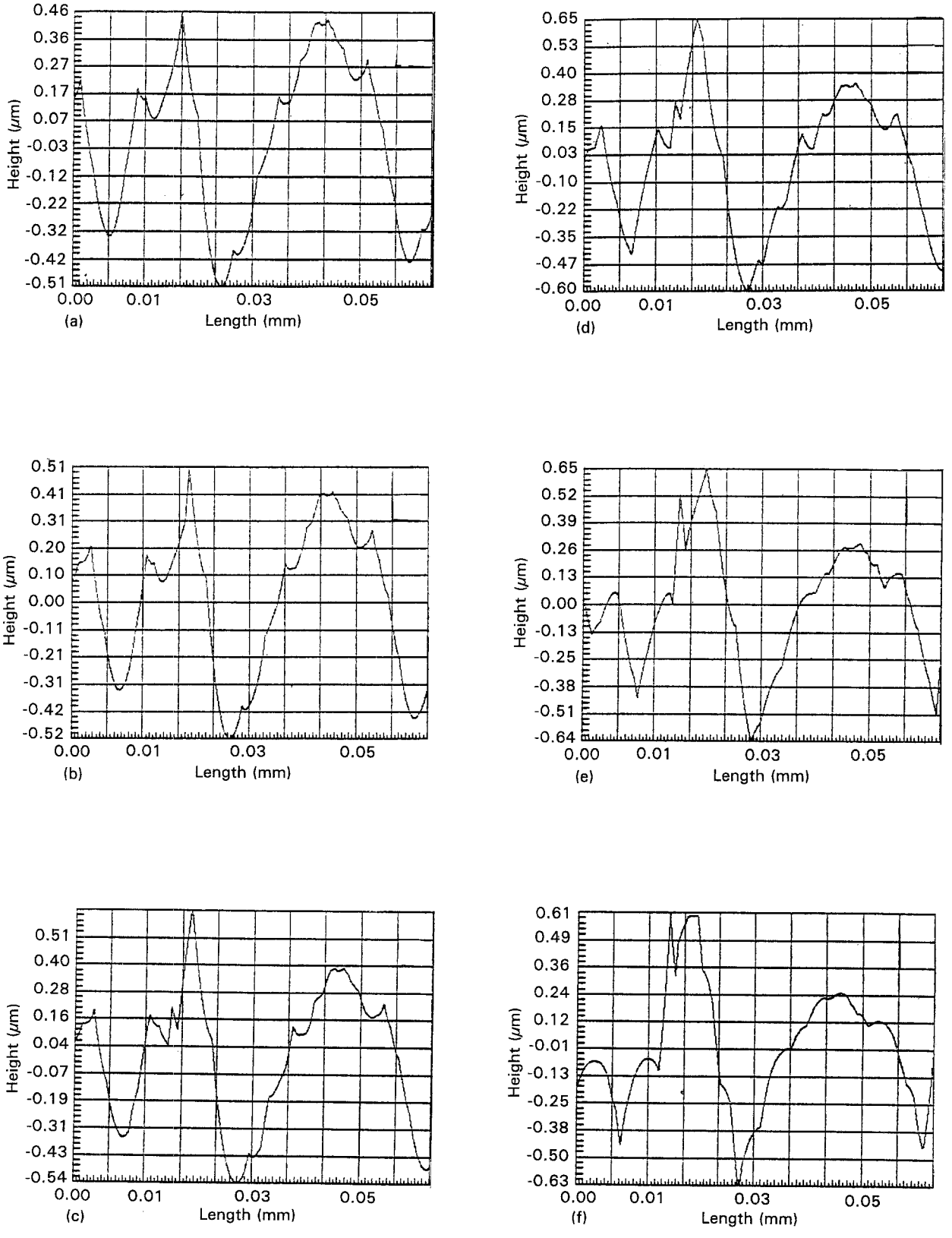

Figure 13 Theoretical changes in the final etched shape (t = 3 arb. units) of x'_1 traces with the angle of cut φ_0. (a–l) are, respectively, for $\varphi_0 = 0°$, 5°, 10°, 14°, 18°, 23°, 26°, 30°, 34°, 37°, 42° and 45°.

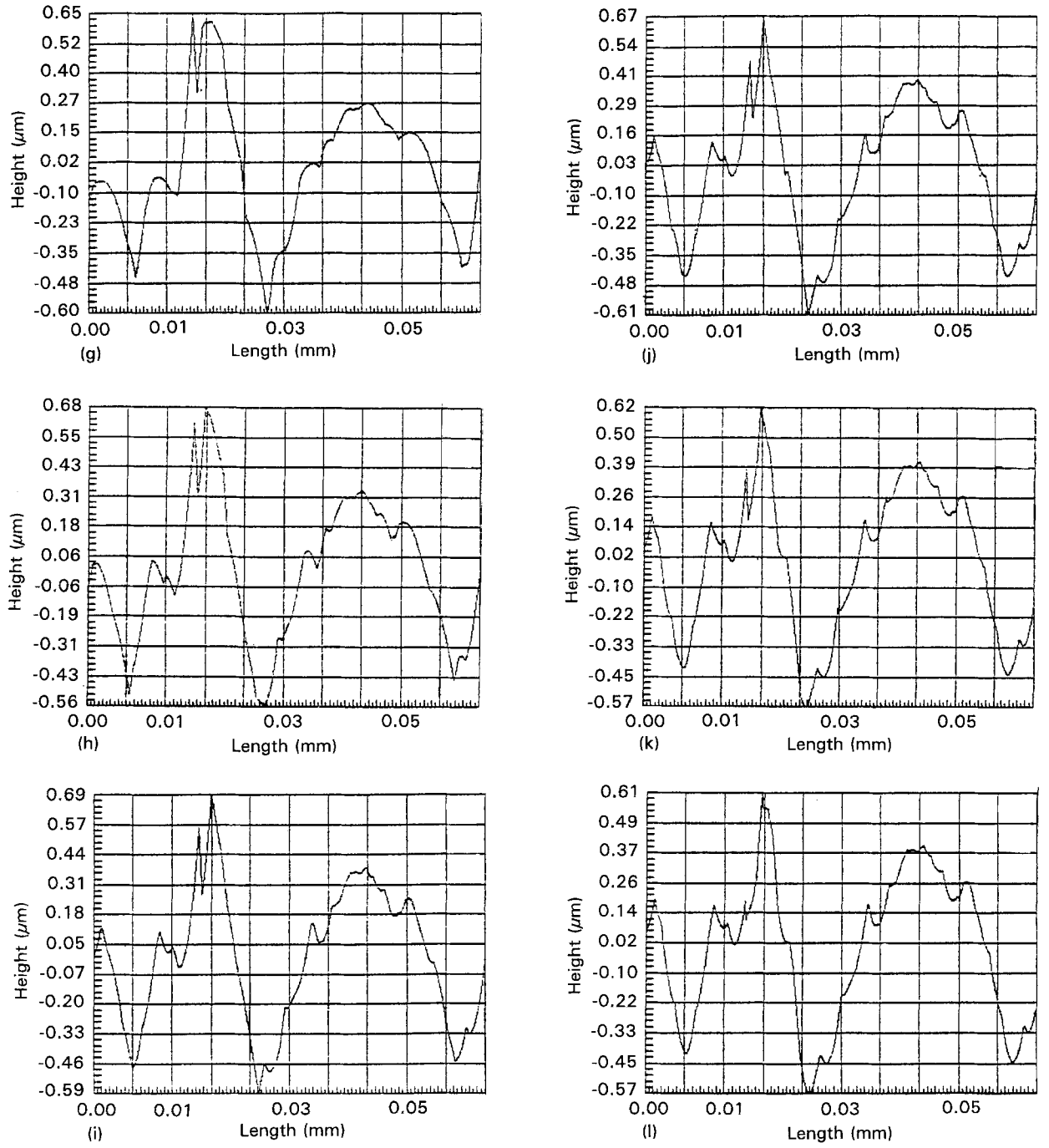

Figure 13 (*Continued*).

TABLE IV Characteristic features of theoretical x' traces as viewed in Fig. 13. The etching time $t = 3$ arb. units (moderately etched surfaces). *A* and *S* indicate "asymmetrical" and "symmetrical", respectively. P_1, P_2, ... correspond to peaks whose angular positions can be easily estimated from distributions of slopes

φ_0 (deg)	Geometrical aspect		Distribution of slopes
	Regions with larger slopes	Regions with smaller slopes	
0	Concave (*S*)	Concave (*S*)	$E_\alpha \approx (-10°, +10°)$; $P_1 \approx 0°$; *S*
5	Rather concave	Rather concave	$E_\alpha \approx (-12°, +8°)$; $P_1 \approx 3°$; *A*
10	Convex–concave	Rather concave	$E_\alpha \approx (-12°, 11°)$; broad peak $P_1 \approx -2°$; *A*
14	Convex–concave	Convex–concave	$E_\alpha \approx (-12°, 12°)$; $P_1 \approx -5°$, $P_2 \approx +5°$; *A*
18	Convex–concave	Convex–concave	$E_\alpha \approx (-13°, +8°)$; $P_1 \approx -8°$, $P_2 \approx 4°$; *A*
23	Convex with some truncations	Convex	$E_\alpha \approx (-16°, 16°)$; $P_1 \approx -0°$; *S*
26	Convex	Convex	$E_\alpha \approx (-12°, 15°)$; $P_1 \approx -2°$; *S*
30	Concave–convex	≈ Concave–convex	$E_\alpha \approx (-24°, 21°)$; $P_1 \approx -6°$; *A*
34	Concave–convex	Concave–convex	$E_\alpha \approx (-10°, 14°)$; broad peak $P_1 \approx -5°$; *A*
37	Concave–convex	Concave–convex	$E_\alpha \approx (-12°, 14°)$; broad peak; *A*
42	Concave–convex	Concave–convex	$E_\alpha \approx (-20°, 22°)$; broad peak $P_1 \approx -5°$; *A*
45	Concave (*S*)	Concave (*S*)	$E_\alpha \approx (-17°, 17°)$; $P_1 \approx 0°$; *S*

force microscope image, it appears that etching causes effectively the formation of curved concave intersections connected with the maximum in L. Thus for {1 1 0} plane, all the features predicted by theory are verified in experiments. Moreover, the influence of the minima minimora ($\varphi_0 = 45°$, $\theta \approx \pm 9°$) can be seen experimentally for cuts φ_0 in the range (30°, 45°) in accord with theory.

In conclusion, the systematic comparison of experimental changes in two-dimensional dissolution shapes on orientation with the theoretical changes cannot allow us to establish any serious disagreement between theory and experiments. Thus, in fact, the shape of the proposed dissolution slowness surface seems rather adequate. A further adjustment of this shape, if necessary, passes through complementary experiments involving three-dimensional shapes, such as those encountered in localized etching at an inert mask. To discuss the adequation of the dissolution surface in terms of experimental shapes related to

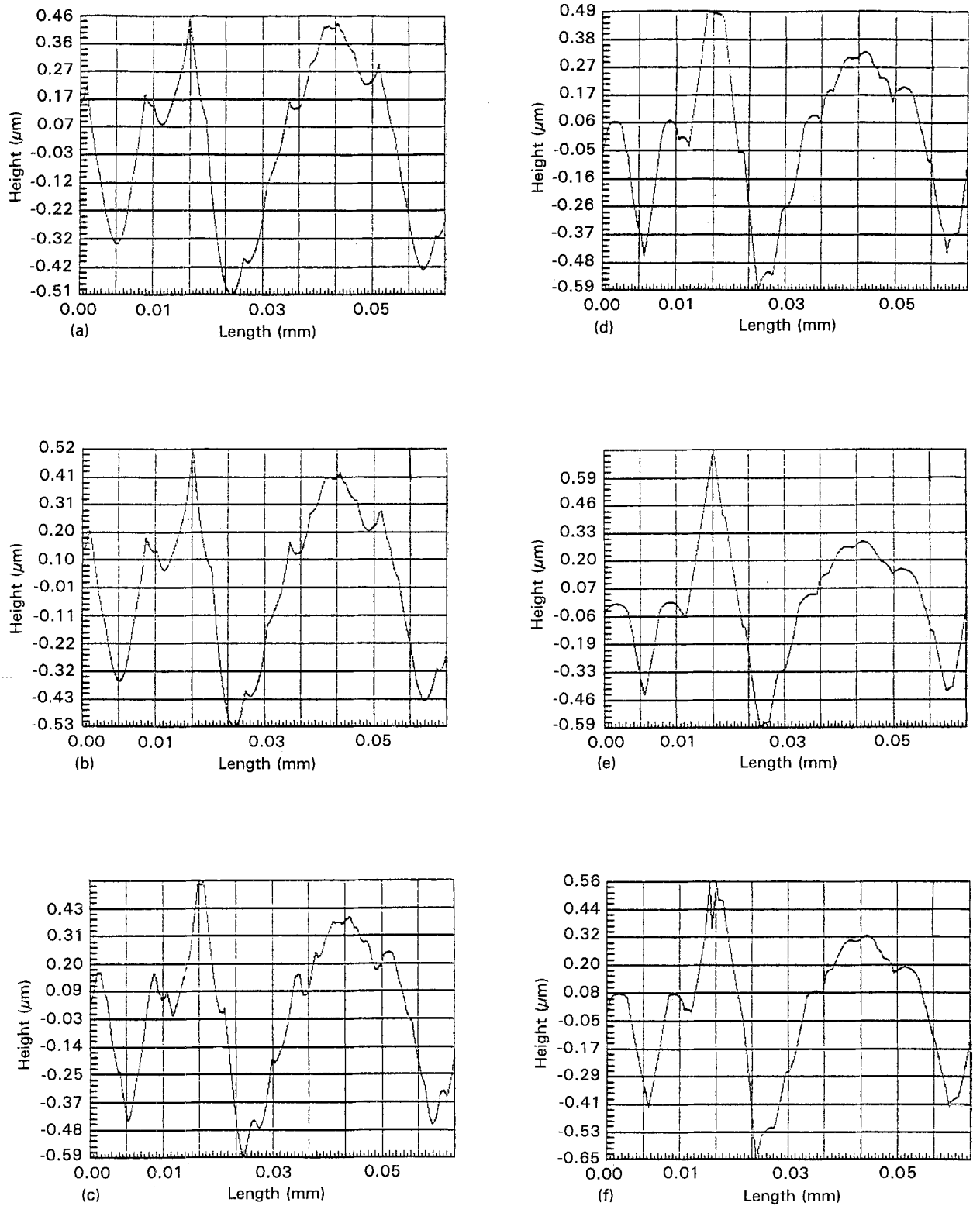

Figure 14 Theoretical changes in the final etched shape (t = 3 arb. units) of [0 0 1] traces with the angle of cut φ_0. (a–l) are, respectively, for $\varphi_0 = 0°$, 5°, 10°, 14°, 18°, 23°, 26°, 30°, 34°, 37°, 42° and 45°.

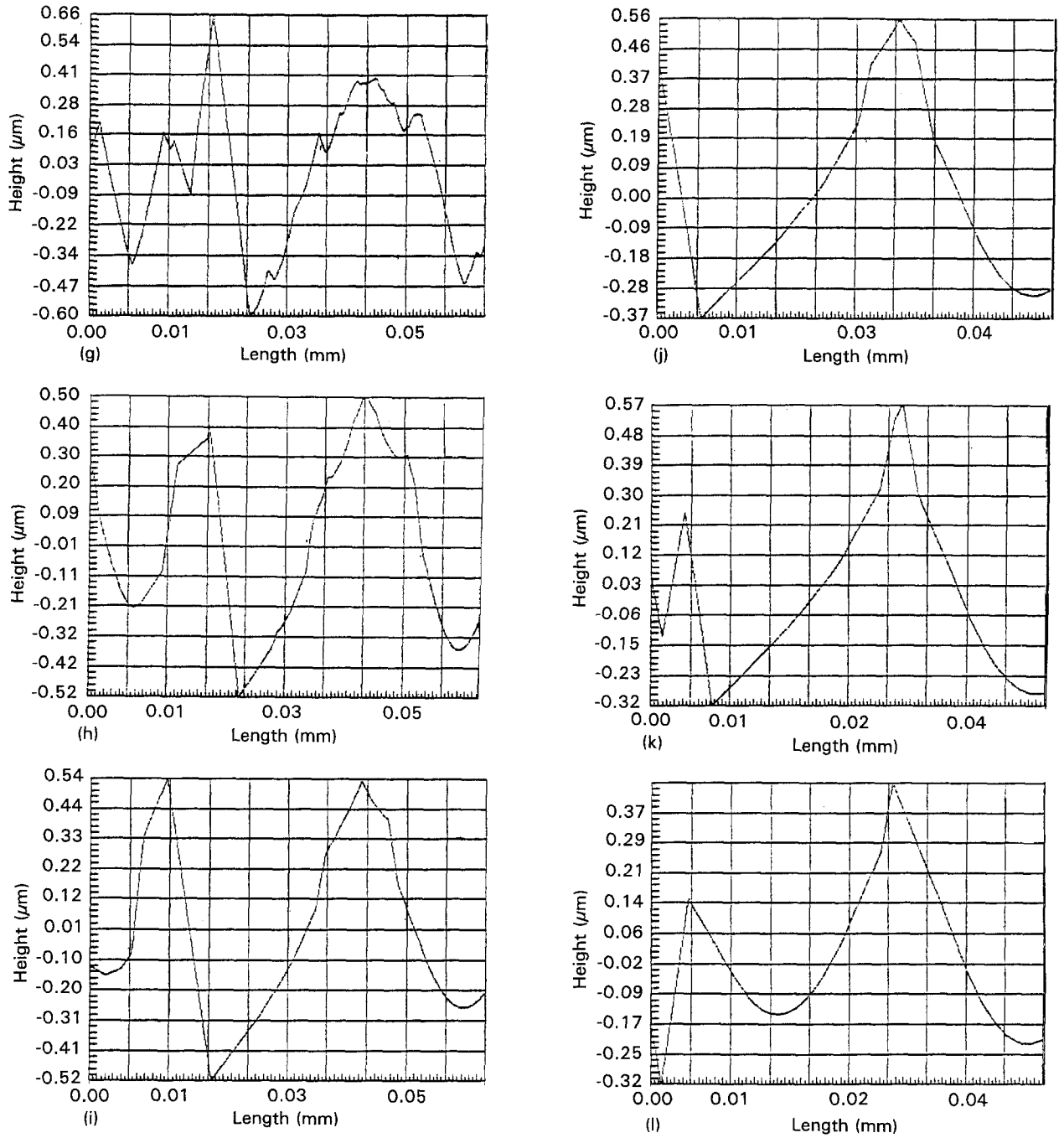

Figure 14 (*Continued*).

TABLE V Characteristic features of theoretical [0 0 1] traces as viewed in Fig. 14. The etching time $t = 3$ arb. units. * Regions with constant slopes. We have indicated in parentheses the angular positions (α_m for a minimum, α_M for a maximum) of extrema in $\boldsymbol{L}$ which generate the geometrical features of etched regions

φ_0 (deg)	Geometrical aspect		Distribution of slopes
	Regions with larger slopes	Regions with smaller slopes	
0	Concave ($\alpha_M = 0°$)	Concave ($\alpha_M = 0°$)	E_α: (− 12°, 12°)
5	Concave ($\alpha_M = 0°$)	Concave ($\alpha_M = 0°$)	E_α: (− 12°, 12°); $\boldsymbol{S}$
10	Concave ($\alpha_M \approx \pm 6$)	Convex ($\alpha_m = 0°$)	E_α: (− 15°, 13°); broad distribution; $\boldsymbol{S}$
14	Concave* ($\alpha_M \approx \pm 10°$)	Convex ($\alpha_m = 0°$)	E_α: (− 14°, 12°); 3 peaks: ≈ − 9°, 0°, ≈ 9°; $\boldsymbol{S}$
18	Concave* ($\alpha_M \approx \pm 10°$)	Convex ($\alpha_m = 0°$)	E_α: (− 13°, 11°); 3 peaks: ≈ − 10°, 0°, ≈ 10°; $\boldsymbol{S}$
23	Concave* ($\alpha_M \approx \pm 8°$); convex ($\alpha_m \approx \pm 16°$)	Convex ($\alpha_m = 0°$)	E_α: (− 31°, 15°); 5 peaks: ≈ − 15°, 8°, 0°, 8°, 15°; $\boldsymbol{S}$
26	Convex* ($\alpha_m \approx \pm 12°$)	Concave ($\alpha_M \approx \pm 4°$), convex ($\alpha_m = 0°$)	E_α: (− 13°, 14°); 3 peaks: − 11°, 0°, 11°; $\boldsymbol{S}$
30	Convex* ($\alpha_m \approx \pm 11°$)	Concave ($\alpha_M = 0°$)	E_α: (− 11°, 9°); 3 peaks: − 10°, 0°, 9°; $\boldsymbol{S}$
34	Convex* ($\alpha_m \approx \pm 9°$)	Concave ($\alpha_M = 0°$)	E_α: (− 10°, 13°); 3 peaks: − 10°, 0°, 9°; $\boldsymbol{S}$
37	Convex* ($\alpha_m \approx \pm 9°$)	Concave ($\alpha_M = 0°$)	E_α: (− 10°, 8°); 3 peaks: − 9°, 0°, 8°; $\boldsymbol{S}$
42	Convex* ($\alpha_m \approx \pm 8°$)	Concave ($\alpha_M = 0°$)	E_α: (− 10°, 8°); 3 peaks: − 9°, 0°, 8°; $\boldsymbol{S}$
45	Convex* ($\alpha_m \approx \pm 8°$)	Concave ($\alpha_M = 0°$)	E_α: (− 8°, 9°); 3 peaks: − 8°, 0°, 9°; $\boldsymbol{S}$

TABLE VI Geometrical features of experimental x' and [001] profilometry traces

φ_0 (deg)	Rotated axis x'	[001] axis
0	Concave and symmetrical	Concave and symmetrical
5	Alternate convex-concave shape (concave regions are more extended)	Concave
10	Alternate convex–concave shape	Convex and symmetrical
14	Alternate convex–concave shape	Convex and symmetrical with stable slopes
18	Alternate convex–concave shape	Convex and symmetrical, stable constant slopes
23	Convex–concave? (rather convex than concave)	Convex and symmetrical
26	Convex	Convex and symmetrical
30	Nearly convex with some concavity for slope $> 10°$	Convex and symmetrical, stable constant slopes
34	Alternate concave–convex shape	Convex and symmetrical
37	Alternate concave–convex shape (convex regions seem more extended)	Convex and symmetrical, stable constant slopes
42	Alternate concave–convex shape	Convex and symmetrical, stable constant slopes
45	Concave and symmetrical	Convex and symmetrical, stable constant slopes

micro-machined structures it becomes necessary to develop a simulation program which allows us to predict shapes for mesa and diaphragms etched into various $(h\,k\,0)$ silicon plates.

We will report experiments on masked $(h\,k\,0)$ plates and tentative attempts to derive theoretical three-dimensional shapes in Part III of this work. We reasonably expect that this future study will contain sufficient information to permit a complete identification of the true shape for the dissolution slowness surface.

References

1. K. SANGWAL, "Etching of Crystals" (North-Holland, Amsterdam, 1987).
2. G. DELAPIERRE, *Sensors Actuators* **17** (1989) 123.
3. F. C. FRANK, in "Growth and Perfection of Crystals", edited by R. H. Doremus, B. W. Robert and D. Turnbull (Wiley, New York, 1965) p. 411.
4. F. C. FRANK and M. B. IVES, *J. Appl. Phys.* **31** (1960) 1996.
5. D. W. SHAW, *J. Electrochem. Soc.* **128** (1981) 874.
6. *Idem, J. Crystal Growth* **47** (1979) 509.
7. C. R. TELLIER, J. Y. AMAUDRUT and A. BRAHIM-BOUNAB, *ibid.* **26** (1991) 595.
8. T. LEBLOIS and C. R. TELLIER, *J. Phys. III* **2** (1992) 1259.
9. A. BRAHIM-BOUNAB and C. R. TELLIER, in "Proceedings of the 6th European Frequency and Time Forum", Noordwijk, The Netherlands, March 1992 (European Space Agency, Paris, 1992) pp. 355–60.

TABLE VII Features revealed by experimental distribution of slopes (etching time $t = 30$ min) related to initially lapped silicon plates. CP, central peak (at $\alpha = 0°$); PP, principal peak; SP, secondary peak; ACP, absence of central peak (at $\alpha = 0°$)

φ_0 (deg)	Rotated x' axis		[001] axis	
	E_α	Features	E_α	Features
0	$(-5°, +5°)$	CP; ***S***	$(-5°, +5°)$	CP; ***S***
5	$(-5°, +11°)$	ACP; ***A***; PP at $\alpha = -2°$; SP at $\alpha = 5°$	$(-10°, +10°)$	CP; ***S***
10	$(-8°, +14°)$	ACP; ***A***; PP at $\alpha = -3°$; SP at $\alpha = 4°$	$(-10°, +10°)$	CP; ***S***
14	$(-11°, 9°)$	ACP; ***A***; PP at $\alpha = -3°$; SP at $\alpha = 5°$	$(-10°, +10°)$	CP; ***S***
18	$(-11°, 9°)$	CP; slightly ***A***	$(-10°, +10°)$	CP; broad and ***S*** distribution
23	$(-7°, 7°)$	CP; ***S***	$(-18°, +18°)$	CP; ***S***
26	$(-11°, +11°)$	CP; slightly ***A***	$(-13°, +13°)$	CP; broad and ***S*** distribution
30	$(-13°, +14°)$	***A***; 2 P at $\alpha = -6°, +4°$	$(-23°, +23°)$	Broad and ***S*** distribution
34	$(-13°, +12°)$	***A; sp*** at $\alpha = -10°$; PP at $\alpha = 3°$	$(-18°, +18°)$	***S***; 2 SP at $\alpha = -9°, +9°$; CP
37	$(-12°)$	ACP; ***A***; 2 P at $\alpha = -7°, +3°$	$(-18°, 16°)$	***S***; 2 SP at $\alpha = -8°, +8°$; CP
42	$(-11°, +5°)$	ACP; ***A***; 2 P at $\alpha = -5°$; PP at $\alpha = 2°$	$(-19°, 19°)$	***S***; broad + 2 SP at $\alpha = -9°, 9°$, CP
45	$(-12°, +12°)$	***S***; Broad	$(-20°, 20°)$	***S***; 2 SP at $\alpha = -9°, +9°$; CP

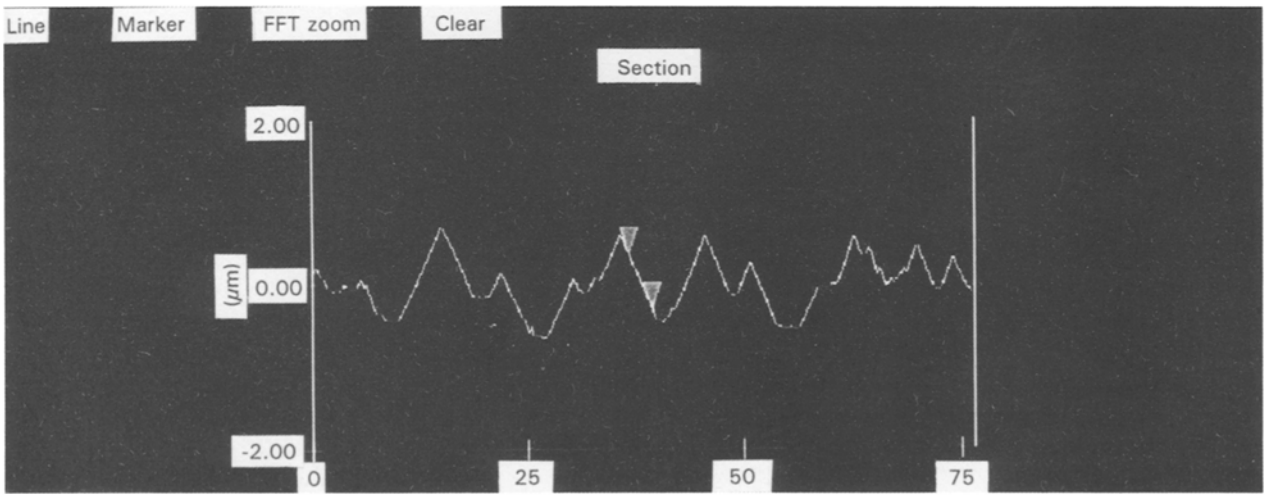

Figure 15 The experimental x_1' profilometry trace as viewed by atomic force microscopy.

10. C. R. TELLIER, T. LEBLOIS, A. BRAHIM-BOUNAB and D. BENMESSAOUDA, in "Proceedings of the 1st Japanese-French Congress of Mecatronique", Besançon, France, October 1992 (Imprimerie du Conseil Général du Doubs, 1992) 6 pp.
11. C. R. TELLIER, T. G. LEBLOIS and P. C. MAITRE, *J. Mater. Sci.* **24** (1989) 3029.
12. J. S. DANEL, F. MICHEL and G. DELAPIERRE, *Sensors Actuators* **A21-A23** (1990) 971.
13. B. W. BATTERMAN, *J. Appl. Phys.* **28** (1957) 1236.
14. M. LIGHTHILL and G. WHITMAN, *Proc. Roy. Soc.* **A229** (1955) 281.
15. C. R. TELLIER and J. L. VATERKOWSKI, *J. Mater. Sci.* **24** (1989) 1077.
16. A. BRAHIM-BOUNAB, J. Y. AMAUDRUT and C. R. TELLIER, *ibid.* **26** (1991) 5585.
17. C. R. TELLIER, *J. Crystal Growth* **100** (1990) 515.
18. C. R. TELLIER, N. VIALLE and J. L. VATERKOWSKI, *Surf. Coat. Technol.* **34** (1988) 417.
19. C. R. TELLIER and A. BRAHIM-BOUNAB, *J. Mater. Sci.* to be published.
20. IEEE "Standard on Piezoelectricity" (IEEE, New York, 1978) p. 15.
21. B. A. IRVING, in "The Electrochemistry of Semiconductors", edited by P. J. Holmes (Academic Press, London, 1962) pp. 256–89.
22. C. R. TELLIER, N. VIALLE and J. L. VATERKOWSKI, in "Proceedings of the 40th Annual Frequency Control Symposium", Philadelphia, PA, May 1986 (IEEE, New York, 1986) pp. 76–85.
23. R. B. HEIMANN, in "Silicon Chemical Etching", edited by J. Grabmaier (Springer, Berlin, 1982).
24. L. CSEPREGI, *Microelectr. Eng.* **3** (1985) 221.
25. K. E. PETERSEN, *Proc. IEEE* **70** (1982) 420.
26. H. SEIDEL, L. CSEPREGI, A. HEUBERGER and H. BAUMGARTEL, *J. Electrochem. Soc.* **137** (1990) 3612.
27. C. R. TELLIER, P. BLIND and D. JOZWICK, in "Proceedings of the 2nd European Frequency and Time Forum", Neuchâtel, Switzerland, March 1988 (Fondation Suisse pour la Recherche en Microtechniques, Neuchâtel, 1988) pp. 937–58.
28. E. G. THWAITE, *Wear* **51** (1978) 253.

Received 7 January
and accepted 5 May 1994